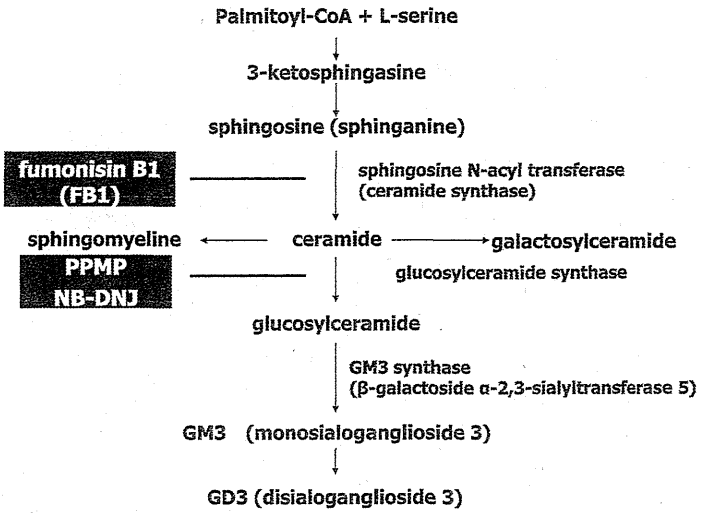

Fig. 1 Pathway of ceramide metabolism

possible interaction with acetic acid, ceramide inhibitors were injected locally with acetic acid by mixing just before the injection.

Determination of the Ceramide Contents in the Stomach

The time-course of changes of the ceramide contents in the stomach was examined. The excised stomachs were cut along the greater curvature and rinsed with physiological saline. Approximately 0.5 g of the tissue sample including the ulcer lesions was removed and minced, and lipid extraction was performed using a modified version of the method described by Bligh and Dyer [24]. After extracting the major lipids, the neutral lipids, including the ceramides, were separated by high-performance thin-layer chromatography (HPTLC) (Silicagel 60, Merck, Germany). The dried lipids were then resolved by thin-layer chromatography using petroleum ether/diethyl ether (7:3) as the first solvent, and chloroform/methanol (95:5) as the second solvent. After separating the lipids, the HPTLC plate was sprayed with a primulin reagent until it was thoroughly wet and then air-dried completely. The lipids were visualized under UV light at 365 nm and analyzed with a densitometer (Fluorchem^{TM} 8000, Alpha Innotech Co., San Leandro, CA, USA). Furthermore, the glucosylceramide and GM3 contents in the stomach were also examined according to the above-mentioned procedure. After the glycosphingolipids were separated by TLC, chloroform/methanol/0.2 % aqueous $CaCl_2$(60/35/8, by volume) was used as the developing agent for the TLC plates. GM3 was visualized by spraying the plate with orcinol-H_2SO_4 reagent. The lipids were visualized under UV light at 365 nm.

Determination of the Degree of Apoptosis in the Gastric Mucosa

Apoptosis was determined by immunohistochemical staining with a polyclonal antibody to ss-DNA. The area of the stomach containing the ulcer was rapidly excised and processed using routine techniques, followed by embedding in paraffin. Sections (4-μm thick) were then prepared and mounted on glass slides. Deparaffinized sections were treated with 3 % hydrogen peroxide for 20 min to block endogenous peroxide. Then, after blocking with 10 % non-immune serum for 10 min at room temperature, the sections were incubated for 40 min at room temperature with a primary antibody (anti-ss-DNA, polyclonal rabbit, DAKO, Carpinteria, CA, USA) diluted 1:100 with 0.1 % bovine serum albumin (BSA) in 0.05 M tris-buffered saline (TBS). The slides were washed three times with 0.05 M TBS-Tween for 5 min, followed by incubation for 30 min with rabbit peroxidase (DAKO). After washing for 5 min in TBS-Tween, the sections were stained using a diaminobenzidine reagent kit (Kirkegaard & Perry Laboratory Inc., Gaithersburg, USA) and observed under a microscope (Nikon ECLIPSE-E-600, Tokyo, Japan). Negative controls containing non-immune rabbit serum with omission of the primary antibody were also prepared. Staining for all antibodies was assessed in a blinded manner by the same observer.

Statistical Analysis

All results were expressed as the mean ± SEM. Differences among groups were evaluated using one-way analysis of variance (ANOVA) and Fisher's post hoc test. Statistical significance was set at $p < 0.05$.

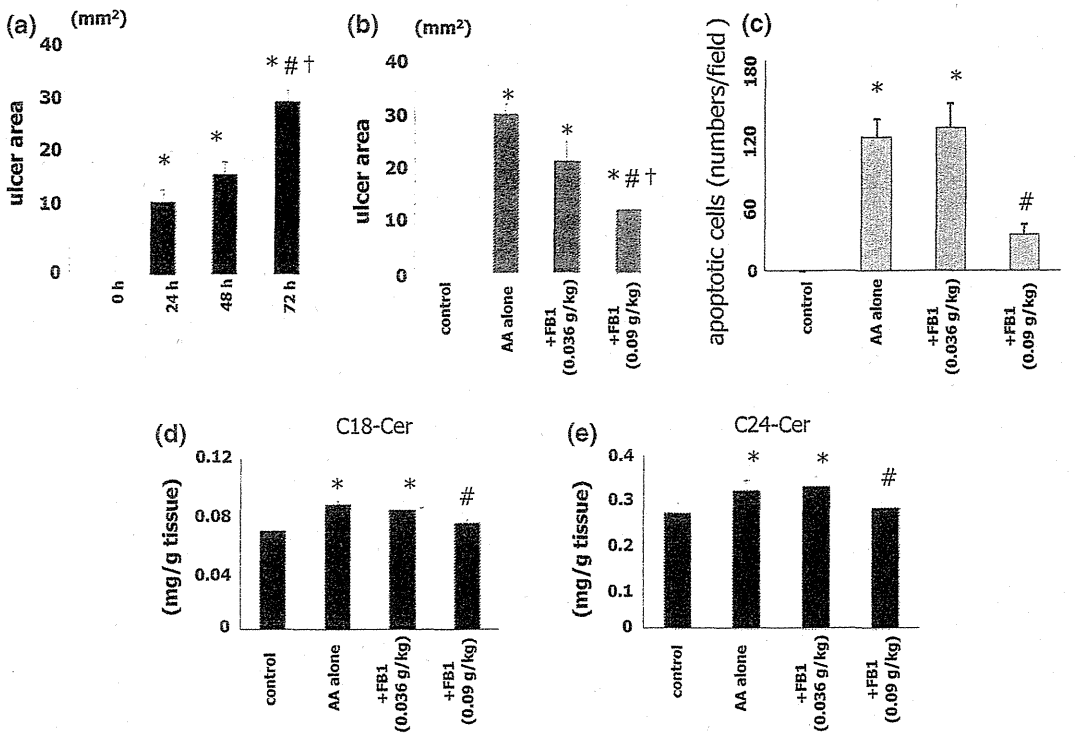

Fig. 2 **a** Time-course of changes in the area of the mucosal lesions after subserosal injection of 20 % acetic acid (50 μl). * $p < 0.05$ vs. 0 h, # $p < 0.05$ vs. 24 h, † $p < 0.05$ vs. 48 h. Each *bar* indicates mean value with SEM of six animals. **b** Inhibitory effects of different concentrations of fumonisin B1 (FB1; 0.036–0.09 g/kg body weight) on acetic acid-induced gastric ulcer formation at 72 h after the injection. Vehicle (water) was injected as a control. The ulcer index is expressed as the area of the mucosal lesions (mm^2). * $p < 0.05$ vs. control. # $p < 0.05$ vs. acetic acid alone. † $p < 0.01$ vs. FB1 (0.036 g/kg body weight). Values are mean ± SEM in six animals. **c** Effects of FB1 on the number of apoptotic cells appearing in the gastric mucosa at 72 h after acetic acid administration. The apoptotic cell number was determined in sections stained immunohistochemically with a polyclonal antibody against ss-DNA, and expressed as the average number of positively stained cells per microscopic field (×400). FB1 at 25 μM significantly attenuated the increase in the number of apoptotic cells induced by acetic acid administration. * $p < 0.05$ vs. control (vehicle); # $p < 0.05$ vs. acetic acid alone. Values are mean ± SEM in six animals. **d**, **e** Ceramide contents in the gastric mucosa at 72 h after acetic acid subserosal injection, and the inhibitory effect of FB1. Four samples were loaded on HPLC plates and densitometric analysis of the C18- (d) and C24- (e) ceramide contents was performed as described in "Materials and Methods". * $p < 0.05$ vs. control. # $p < 0.05$ vs. acetic acid alone. Values are mean ± SEM in six animals

Results

Effect of Fumonisin B1 on Acetic Acid-Induced Ulcer Formation

Figure 2a shows the time-course of changes in the area of the mucosal lesions, and Fig. 2b shows the inhibitory effects of different concentrations of fumonisin B1 (FB1; 0.036 and 0.09 g/kg body weight) on the area of the lesions after 72 h. The ulcers produced by the acetic acid injection began to form at the injection site in the stomach, expanded to their maximum size after 72 h, and healed gradually from day 5 to day 8 (data not shown). The ulcer formation was significantly inhibited by FB1 at the dose of 0.09 g/kg.

Figure 2c shows the number of apoptotic cells in the gastric mucosa at 72 h after the acetic acid injection as assessed immunohistochemically by light microscopy. A significant increase in the number of apoptotic cells was observed at 72 h after the acetic acid injection. FB1 at 0.036 g/kg did not significantly inhibit the acetic acid-induced apoptosis at 72 h, but the drug at 0.09 g/kg significantly attenuated the increase in the frequency of apoptosis induced by acetic acid at 72 h, which is consistent with the inhibition of ulcer formation by the drug. Figure 2d, e shows the C18- (2d) and C24- (2e) ceramide contents in the gastric mucosal lesions at 72 h after the acetic acid injection, and the inhibitory effect of FB1 on the accumulation of ceramides. The amounts of both the C18 and C24 ceramide were significantly increased at 72 h after the acetic acid injection, but not at 24 or 48 h after the injection (data not shown). The increase in the contents of the C18 and C24 ceramides in response to acetic acid injection was significantly attenuated by co-injection of FB1 (0.09 g/kg).

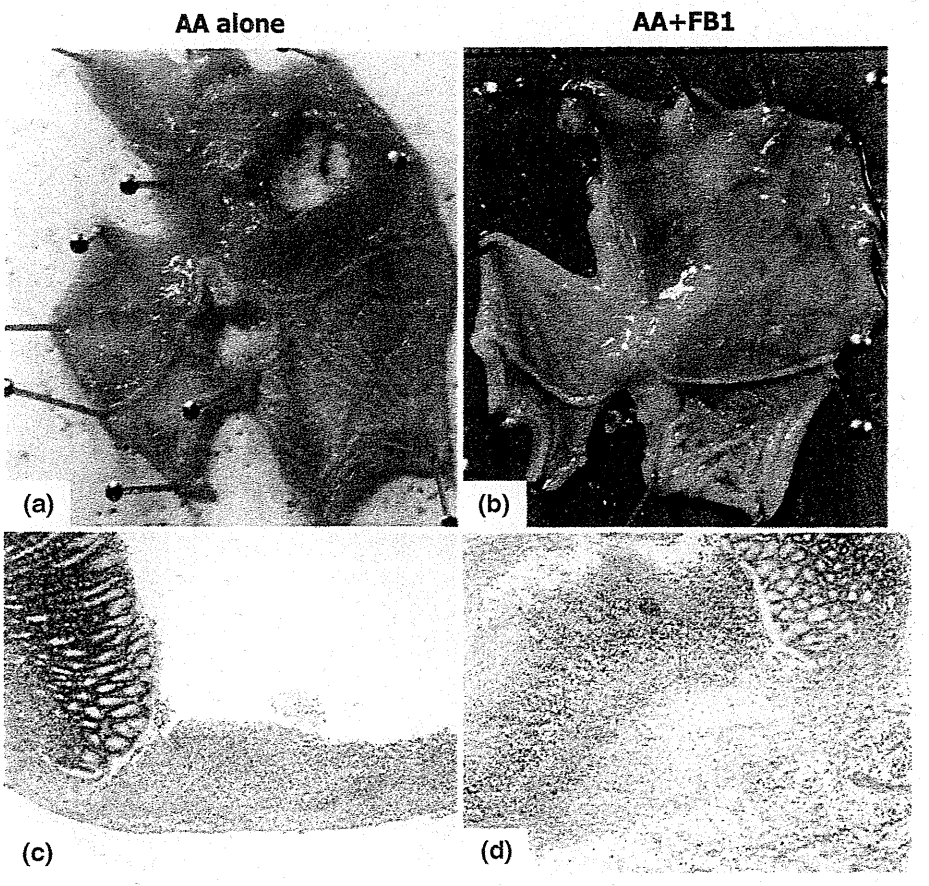

Fig. 3 Representative macroscopic findings were shown. **a** Acetic acid-induced gastric ulcer 72 h after subserosal injection. **b** Acetic acid-induced ulcer formation 72 h after subserosal injection was attenuated by the application of fumonisin B1 (0.09 g/kg body weight). **c**, **d** Representative hematoxylin-eosin (H&E)-stained histopathological findings were shown. **c** Acetic acid-induced ulcer 72 h after subserosal injection (×10). **d** Acetic acid-induced ulcer 72 h after subserosal injection was attenuated by fumonisin B1 (0.09 g/kg body weight) application (×10)

Figure 3a shows the representative macroscopic findings of acetic acid (AA)-induced gastric ulcer. As shown in Fig. 3b, AA-induced ulcer formation was attenuated by the application of FB1. Figure 3c shows the representative histopathological (hematoxylin-eosin staining) finding of AA-induced ulcer. As in Fig. 3d, such AA-induced-ulcer was attenuated by FB1 application.

Effect of PPMP on Acetic Acid-Induced Ulcer Formation

Figure 4a shows the effect of the glucosylceramide synthase inhibitor, PPMP, on acetic acid-induced gastric ulcer formation. PPMP at concentrations of over 0.127 g/kg body weight attenuated the sizes of the acetic acid-induced gastric mucosal lesions at 72 h after treatment.

Figure 4b shows the effect of PPMP on the number of apoptotic cells in the gastric mucosa at 72 h after acetic acid injection. Co-injection of PPMP with acetic acid at doses of over 0.127 g/kg significantly inhibited the acetic acid-induced increase in the number of apoptotic cells which is consistent with the inhibition of ulcer formation by the drug. Figure 4c, d shows a quantitative analysis of the contents of the C18- (4c) and C24- (4d) ceramide after acetic acid injection and the effect of PPMP. The increase in the amounts of both the C18- and C24-ceramide observed at 72 h after acetic acid injection was further enhanced by the concomitant injection of PPMP, and significantly greater amounts of the ceramides were found in the lesions following injection of PPMP at doses higher than 0.127 g/kg.

Effect of NB-DNJ on Acetic Acid-Induced Ulcer Formation

Figure 5a shows the effect of another glucosylceramide synthase inhibitor, NB-DNJ, on acetic acid-induced gastric ulcer formation. Co-injection of NB-DNJ with acetic acid at doses of over 1.1 g/kg body weight significantly attenuated the formation of the gastric mucosal lesions observed at 72 h after the acetic acid injection. Figure 5b shows the effect of NB-DNJ on the number of apoptotic cells appearing in the gastric mucosa at 72 h after the acetic acid injection. Co-injection of NB-DNJ at doses of over 0.11 g/kg body weight significantly attenuated the acetic acid-induced apoptosis in the gastric mucosa. Figure 5c, d shows the effect of NB-DNJ on the contents of the C18- (5c) and C24- (5d) ceramide at 72 h after acetic acid injection. The C18- and C24-ceramide contents significantly increased following

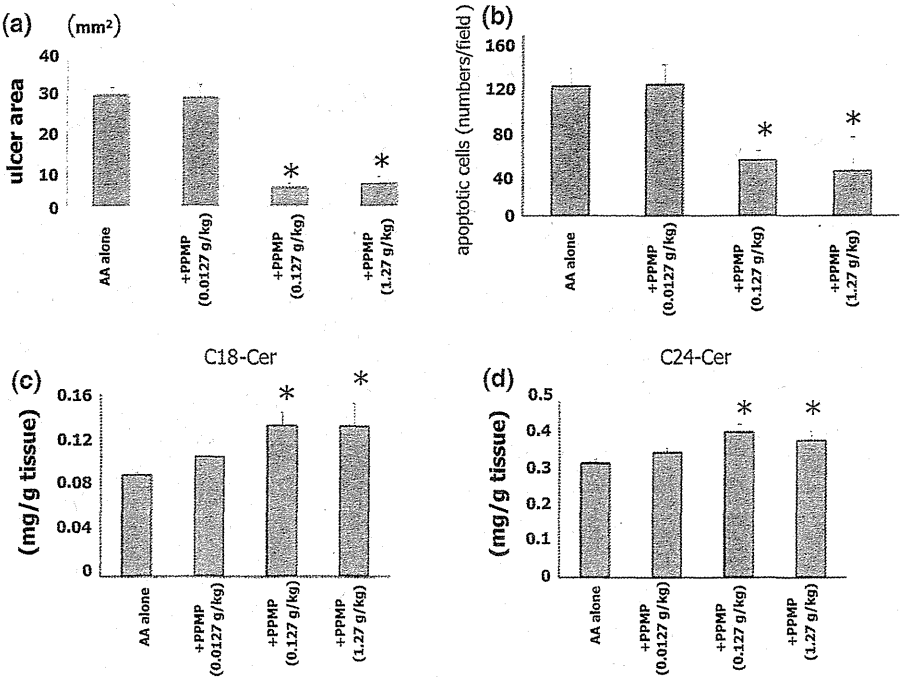

Fig. 4 Each *bar* indicates mean value with SEM of six animals. **a** Effect of the glucosylceramide synthase inhibitor, PPMP, on acetic acid-induced gastric ulcer formation at 72 h after treatment. PPMP (0.0127–1.27 g/kg body weight) was injected concomitantly with acetic acid into the gastric subserosa. * $p < 0.05$ vs. acetic acid alone. Values are mean ± SEM in six animals. **b** Effect of PPMP on the number of apoptotic cells appearing in the gastric mucosa at 72 h after acetic acid administration. PPMP (0.0127–1.27 g/kg body weight) was injected concomitantly with acetic acid into the gastric subserosa. * $p < 0.05$ vs. acetic acid alone. **c**, **d** C18- (c) and C24- (d) ceramide contents observed in the gastric mucosa at 72 h after acetic acid administration. PPMP (0.0127–1.27 g/kg body weight) was injected concomitantly with acetic acid into the gastric subserosa. * $p < 0.05$ vs. acetic acid alone. Values are mean ± SEM in six animals

co-injection of NB-DNJ (1.1 g/kg body weight) as compared with that observed following the injection of acetic acid alone, reflecting the decreased conversion of ceramide to glycosylceramide in these situations.

Glucosylceramide and GM3 on Acetic Acid-Induced Ulcer Formation

Figure 6 shows glucosylceramide and GM3 expressions in acetic acid-induced ulcer formation. The glucosylceramide levels were remarkably low in the acetic acid-induced ulcer group than in the control group. The level of ganglioside GM3 was observed to be high in the acetic acid-induced ulcer group. The expression of GM3 was suppressed and that of glucosylceramide were not restored by the treatment with glucosylceramide synthase inhibitors (PPMP, NB-DNJ).

Discussion

Our present results showing that the blockade of ceramide synthase by fumonisin B1 attenuates acetic acid-induced gastric ulcer formation suggest the importance of de novo ceramide synthesis in the process of ulcer formation induced by acetic acid. Although ceramides, which are derived from the hydrolysis of sphingomyelin in response to extracellular signals, appear to be important in most pathways [10], ceramide synthase-mediated processes, such as the acylation of sphinganine in the de novo biosynthetic pathway of sphingolipids as well as the reutilization of sphingosine derived from sphingolipid turnover [23, 25] may mainly account for the bioactive roles of ceramides in ulcer formation. In this study, we demonstrated an increase in the number of apoptotic cells in the gastric mucosa at 3 h after the injection of acetic acid, with subsequent extension of the lesion area containing apoptotic cells toward the submucosa, as well as a significant attenuation of the increase in acetic acid-induced apoptosis by co-injection of fumonisin B1. These findings suggest that the ceramide pathway may account for the acetic acid-induced ulcer formation via enhancing apoptotic cell death in the damaged mucosa. Our results also confirmed the significant role of the ceramide pathway in other specific experimental models of ulcers, such as PMA-induced gastric ulcers, besides that in the prototype model, namely, the model of acetic acid-induced ulcer [22].

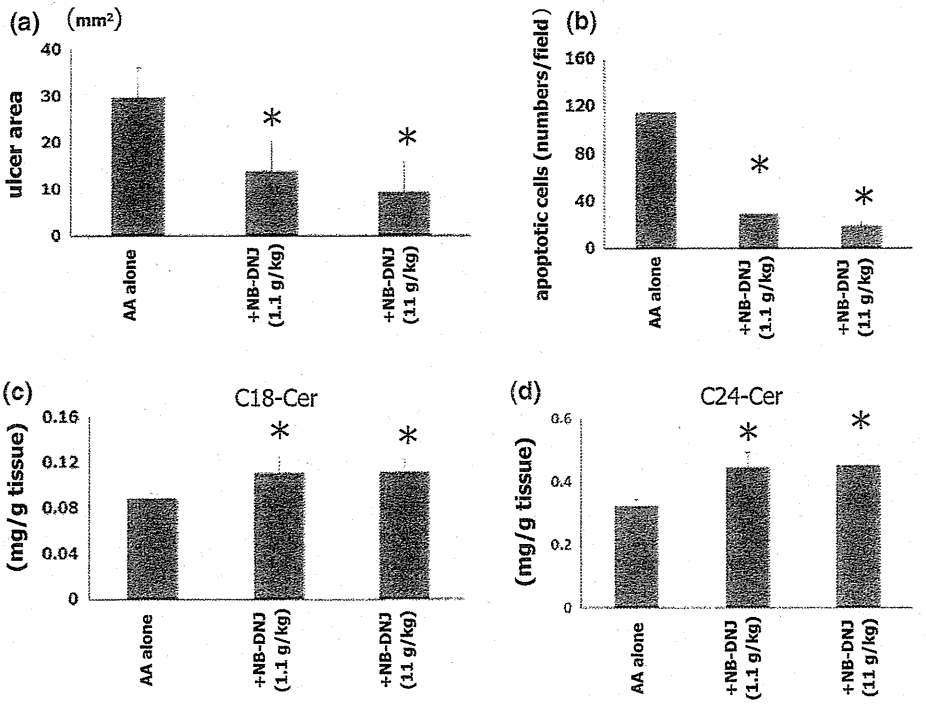

Fig. 5 Each *bar* indicates mean value with SEM of six animals. **a** Effect of NB-DNJ on acetic acid-induced gastric ulcer formation at 72 h after NB-DNJ (0.11–11 g/kg body weight) concomitant administration of the NB-DNJ with acetic acid into the gastric subserosa. * $p < 0.05$ vs. acetic acid alone. Values are the mean ± SEM in six animals. **b** Effect of NB-DNJ on the number of apoptotic cells appearing in the gastric mucosa at 72 h after acetic acid administration. NB-DNJ (0.11–11 g/kg body weight) was injected concomitantly with acetic acid into the gastric subserosa. * $p < 0.05$ vs. acetic acid alone. **c, d** Effect of NB-DNJ on the C18- (c) and C24- (d) ceramide contents observed in the gastric mucosa at 72 h after acetic acid administration. NB-DNJ (0.11–11 g/kg body weight) was injected concomitantly with acetic acid into the gastric subserosa. * $p < 0.05$ vs. acetic acid alone. Values are mean ± SEM in six animals

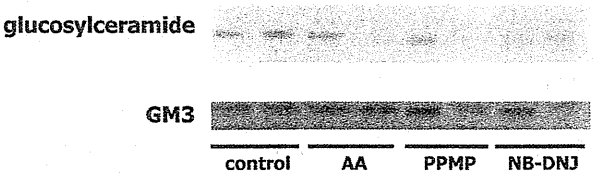

Fig. 6 Effect of PPMP (1.27 g/kg body weight) and NB-DNJ (11 g/kg body weight) on the glucosylceramide and GM3 after subserosal injection of 20 % acetic acid (50 µl). Representative pictures of thin layer chromatography of the glucosylceramide (*upper*) and GM3 (*lower*). Control: H_2O (sterile water) injection

In the present study, we demonstrated that the product of glucosylceramide synthase and not a ceramide itself induces apoptosis, and thus, glucosylceramide synthase inhibitors will decrease apoptosis. The reason for this decrease might be that apoptosis is induced by the product of glucosylceramide synthase.

In our previous manuscript [18], we only examined the increase in the ceramide (C18, C24) levels; we did not evaluate the levels of the ceramide metabolites. However, we showed that the increase in apoptosis in the gastric mucosa corresponded with the increase in the levels of C18 and C24 ceramide in the stomach wall, and that apoptosis was involved in the formation of gastric ulcers induced by PMA (phorbol 12-myristate 13-acetate). Although we previously suggested that ceramide or ceramide metabolites could be ulcerogenic [18], which of the two is ulcerogenic was not determined. In this context, in the previous study, a possibility that ceramide or ceramide metabolites could be a cause of ulcers was established. Our present results indicated that it is neither the C18- nor the C24-ceramide itself, but the respective metabolites that may be ulcerogenic, because we found, to our surprise, that glucosylceramide synthase inhibitors that reduce the degradation of ceramide can also attenuate the gastric mucosal damage induced by acetic acid. We used two types of inhibitors, namely, PPMP, a synthetic inhibitor of glucosylceramide synthase [26] and NB-DNJ, an N-alkylated imino sugar that blocks the activity of ceramide-specific glucosyltransferase which catalyzes the formation of glucosylceramide [27], both of which inhibit the conversion of ceramide to glucosylceramide. Indeed, the contents of the C18- and C24-ceramides were significantly augmented in the gastric mucosa when these inhibitors were injected

concomitantly with acetic acid. On the other hand, the acetic acid-induced tissue damage was attenuated with a decrease in the number of apoptotic cells under this condition, suggesting that inhibition of the synthesis of glucosylceramide, a precursor for neutral glycosphingolipids and gangliosides, effectively inhibits ulcer formation.

In the group of acetic acid-induced ulcer, while the glucosylceramide was not increased, the GM3 was remarkably accumulated as compared with the control group, suggesting that ceramide seems to be rapidly metabolized to ganglioside GM3 without accumulating intermediate metabolite such as glucosylceramide. On the other hand, in the group of acetic acid-induced ulcer treated with glucosylceramide synthesis inhibitors, the levels of both glucosylceramide and GM3 were not restored to the control level because glucosylceramide synthesis inhibitors could attenuate the pathway upstream of the glucosylceramide.

In the present study, we examined only the glucosylceramide pathway, and not the other pathways such as the sphingomyelin pathway. According to previous reports, GD3, a downstream metabolite of ceramide, is a key signaling intermediate leading to apoptosis [28], and the recently characterized trafficking of ganglioside GD3 to the mitochondria has revealed a novel function of this lipid as a death effector [29]; thus, the glucosylceramide pathway would be the main pathway, which is co-localized with the other pathways such as the sphingomyelin pathway.

Glucosylceramide synthase is a constitutively expressed type III integral membrane protein on the cytosolic side of the *cis/medial* Golgi membrane [30]. After its translocation to the Golgi lumen by an as yet undefined signaling mechanism, glucosylceramide is further metabolized to higher glycosphingolipids, including GM3 and GD3 gangliosides [11, 31]. It has been suggested previously that glycosylation of ceramide can protect cells from cancer drug-induced apoptosis. Accumulation of glucosylceramide was observed in multidrug-resistant tumor cells [32], and overexpression of glucosylceramide synthase in MCF-7 breast cancer cells conferred resistance to adriamycin and TNF-α [33]. These findings would support the idea that glycosylation of ceramide rather attenuates its capacity to act as a second messenger in apoptosis, although recently, it has been suggested that the natural ceramide species accumulating during the execution phase of apoptosis are not converted by glucosylceramide synthase to glucosylceramide, because this pool of ceramide is topologically segregated from glucosylceramide synthase [11]. In any event, the glucosylceramide formation *per se* does not appear to be a potentially toxic mediator in the acetic acid-induced gastric damage.

In addition to their role in the regulation of apoptosis, ceramides also provide the carbon backbone for the synthesis of complex glycosphingolipids within the Golgi network [34]. Inhibitors of glycosphingolipid biosynthesis have been used successfully as therapeutic agents for glycosphingolipid lysosomal storage diseases [35]. Healthy mice treated with NB-DNJ exhibited 70 % peripheral glycosphingolipid depletion [36], and clinical trials have shown the efficacy of these agents in patients with type 1 Gaucher's disease [37]. In addition, recently, ganglioside GD3 (GD3), a sialic acid-containing glycosphingolipid, has attracted considerable attention due to its emerging role as an effector of cell death by activating the mitochondrial-dependent apoptosis through sequential membrane permeability transition induction, cytochrome c release, and caspase activation [38]. De Maria et al. [39] showed that GD3 ganglioside mediates the propagation of CD95 (Fas)-generated apoptotic signals in hematopoietic cells, and that the pharmacological inhibition of GD3 synthesis and exposure to GD3 synthase antisense oligonucleotides prevented CD95-induced apoptosis. Another group recently demonstrated that the inhibition of glucosylceramide synthase, which blunted TNF-stimulated GD3 levels, abolished TNF-mediated apoptosis in human colon cancer cells [40], and also that *d-threo*-PDMP, an inhibitor of glucosylceramide synthase, blocked the TNF-α-induced translocation of GD3 to the mitochondria, thereby preserving its predominant localization at the cell surface in rat hepatocytes [41]. Since we previously demonstrated that an antibody against TNF-α significantly inhibited ulcer formation in the PMA-induced gastric ulcer model [17], TNF-α may also be involved in the process of acetic acid-induced ulcer formation. These previous reports suggesting that GD3 may play a significant role in TNF-α-mediated apoptosis are in close concordance with our present data indicating that inhibitors of glucosylceramide synthase successfully prevented the apoptosis and ulcer formation induced by acetic acid in spite of the significant accumulation of ceramide content observed in the gastric tissues.

Acknowledgments This study was supported by a Grant-in-Aid for Scientific Research (B) from the Japan Society for the Promotion of Science (22300169, to H.S.), Grant-in-Aid for challenging Exploratory Research (24659103, to H.S.), a grant from the National Defense Medical College (to S.M.), a Research Fund of Mitsukoshi Health and Welfare Foundation (to H.S.), and a grant from the Smoking Research Foundation (to H.S.).

Conflict of interest None.

References

1. Konturek PC, Brzozowski T, Konturek SJ, et al. Apoptosis in gastric mucosa with stress-induced gastric ulcers. *J Physiol Pharmacol.* 1999;50:211–225.
2. Suzuki H, Ishii H. Role of apoptosis in *Helicobacter pylori*-associated gastric mucosal injury. *J Gastroenterol Hepatol.* 2000;15:D46–D54.

3. Suzuki H, Hibi T, Marshall BJ. *Helicobacter pylori*: present status and future prospects in Japan. *J Gastroenterol.* 2007;42: 1–15.
4. Suzuki H, Marshall BJ, Hibi T. Overview: *Helicobacter pylori* and extragastric disease. *Int J Hematol.* 2006;84:291–300.
5. Suzuki H, Iwasaki E, Hibi T. *Helicobacter pylori* and gastric cancer. *Gastric Cancer.* 2009;12:79–87.
6. Leung WK, To KF, Chan FK, Lee TL, Chung SC, Sung JJ. Interaction of *Helicobacter pylori* eradication and non-steroidal anti-inflammatory drugs on gastric epithelial apoptosis and proliferation: implications on ulcerogenesis. *Aliment Pharmacol Ther.* 2000;14:879–885.
7. Nagata H, Akiba Y, Suzuki H, Okano H, Hibi T. Expression of Musashi-1 in the rat stomach and changes during mucosal injury and restitution. *FEBS Lett.* 2006;580:27–33.
8. Liu ES, Cho CH. Relationship between ethanol-induced gastritis and gastric ulcer formation in rats. *Digestion.* 2000;62:232–239.
9. Hakomori S, Igarashi Y. Functional role of glycosphingolipids in cell recognition and signaling. *J Biochem (Tokyo).* 1995;118: 1091–1103.
10. Hannun YA. Functions of ceramide in coordinating cellular responses to stress. *Science.* 1996;274:1855–1859.
11. Tepper AD, Diks SH, van Blitterswijk WJ, Borst J. Glucosylceramide synthase does not attenuate the ceramide pool accumulating during apoptosis induced by CD95 or anti-cancer regimens. *J Biol Chem.* 2000;275:34810–34817.
12. Obeid LM, Linardic CM, Karolak LA, Hannun YA. Programmed cell death induced by ceramide. *Science.* 1993;259:1769–1771.
13. Dbaibo GS, Obeid LM, Hannun YA. Tumor necrosis factor-α (TNF-α) signal transduction through ceramide. Dissociation of growth inhibitory effects of TNF-α from activation of nuclear factor-kappa B. *J Biol Chem.* 1993;268:17762–17766.
14. Kolesnick R, Golde DW. The sphingomyelin pathway in tumor necrosis factor and interleukin-1 signaling. *Cell.* 1994;77: 325–328.
15. Kim MY, Linardic C, Obeid L, Hannun Y. Identification of sphingomyelin turnover as an effector mechanism for the action of tumor necrosis factor α and γ-interferon. Specific role in cell differentiation. *J Biol Chem.* 1991;266:484–489.
16. Cifone MG, De Maria R, Roncaioli P, et al. Apoptotic signaling through CD95 (Fas/Apo-1) activates an acidic sphingomyelinase. *J Exp Med.* 1994;180:1547–1552.
17. Takeuchi T, Miura S, Wang L, et al. Nuclear factor-kappa B and TNF-α mediate gastric ulceration induced by phorbol myristate acetate. *Dig Dis Sci.* 2002;47:2070–2078.
18. Uehara K, Miura S, Takeuchi T, et al. Significant role of ceramide pathway in experimental gastric ulcer formation in rats. *J Pharmacol Exp Ther.* 2003;305:232–239.
19. Koltun E, Richards S, Chan V, et al. Discovery of a new class of glucosylceramide synthase inhibitors. *Bioorg Med Chem Lett.* 2011;21:6773–6777.
20. Shayman JA, Lee L, Abe A, Shu L. Inhibitors of glucosylceramide synthase. *Methods Enzymol.* 2000;311:373–387.
21. Platt FM, Neises GR, Karlsson GB, Dwek RA, Butters TD. N-butyldeoxygalactonojirimycin inhibits glycolipid biosynthesis but does not affect N-linked oligosaccharide processing. *J Biol Chem.* 1994;269:27108–27114.
22. Okabe S, Pfeiffer CJ. Chronicity of acetic acid ulcer in the rat stomach. *Am J Dig Dis.* 1972;17:619–629.
23. Wang E, Norred WP, Bacon CW, Riley RT, Merrill AH Jr. Inhibition of sphingolipid biosynthesis by fumonisins. Implications for diseases associated with Fusarium moniliforme. *J Biol Chem.* 1991;266:14486–14490.
24. Berg H, Magard M, Johansson G, Mathiasson L. Development of a supercritical fluid extraction method for determination of lipid classes and total fat in meats and its comparison with conventional methods. *J Chromatogr A.* 1997;785:345–352.
25. Merrill AH Jr, van Echten G, Wang E, Sandhoff K. Fumonisin B1 inhibits sphingosine (sphinganine) N-acyltransferase and de novo sphingolipid biosynthesis in cultured neurons in situ. *J Biol Chem.* 1993;268:27299–27306.
26. Maurer BJ, Melton L, Billups C, Cabot MC, Reynolds CP. Synergistic cytotoxicity in solid tumor cell lines between N-(4-hydroxyphenyl)retinamide and modulators of ceramide metabolism. *J Natl Cancer Inst.* 2000;92:1897–1909.
27. Svensson M, Frendeus B, Butters T, Platt F, Dwek R, Svanborg C. Glycolipid depletion in antimicrobial therapy. *Mol Microbiol.* 2003;47:453–461.
28. Lovat PE, Corazzari M, Di Sano F, Piacentini M, Redfern CP. The role of gangliosides in fenretinide-induced apoptosis of neuroblastoma. *Cancer Lett.* 2005;228:105–110.
29. Morales A, Colell A, Mari M, Garcia-Ruiz C, Fernandez-Checa JC. Glycosphingolipids and mitochondria: role in apoptosis and disease. *Glycoconj J.* 2004;20:579–588.
30. Jeckel D, Karrenbauer A, Burger KN, van Meer G, Wieland F. Glucosylceramide is synthesized at the cytosolic surface of various Golgi subfractions. *J Cell Biol.* 1992;117:259–267.
31. Ichikawa S, Hirabayashi Y. Glucosylceramide synthase and glycosphingolipid synthesis. *Trends Cell Biol.* 1998;8:198–202.
32. Lavie Y, Cao H, Bursten SL, Giuliano AE, Cabot MC. Accumulation of glucosylceramides in multidrug-resistant cancer cells. *J Biol Chem.* 1996;271:19530–19536.
33. Liu YY, Han TY, Giuliano AE, Ichikawa S, Hirabayashi Y, Cabot MC. Glycosylation of ceramide potentiates cellular resistance to tumor necrosis factor-α-induced apoptosis. *Exp Cell Res.* 1999;252:464–470.
34. Kolter T, Proia RL, Sandhoff K. Combinatorial ganglioside biosynthesis. *J Biol Chem.* 2002;277:25859–25862.
35. Platt FM, Neises GR, Reinkensmeier G, et al. Prevention of lysosomal storage in Tay-Sachs mice treated with N-butyldeoxynojirimycin. *Science.* 1997;276:428–431.
36. Platt FM, Reinkensmeier G, Dwek RA, Butters TD. Extensive glycosphingolipid depletion in the liver and lymphoid organs of mice treated with N-butyldeoxynojirimycin. *J Biol Chem.* 1997;272:19365–19372.
37. Cox T, Lachmann R, Hollak C, et al. Novel oral treatment of Gaucher's disease with N-butyldeoxynojirimycin (OGT 918) to decrease substrate biosynthesis. *Lancet.* 2000;355:1481–1485.
38. Garcia-Ruiz C, Colell A, Paris R, Fernandez-Checa JC. Direct interaction of GD3 ganglioside with mitochondria generates reactive oxygen species followed by mitochondrial permeability transition, cytochrome c release, and caspase activation. *FASEB J.* 2000;14:847–858.
39. De Maria R, Lenti L, Malisan F, et al. Requirement for GD3 ganglioside in CD95- and ceramide-induced apoptosis. *Science.* 1997;277:1652–1655.
40. Colell A, Morales A, Fernandez-Checa JC, Garcia-Ruiz C. Ceramide generated by acidic sphingomyelinase contributes to tumor necrosis factor-α-mediated apoptosis in human colon HT-29 cells through glycosphingolipids formation. Possible role of ganglioside GD3. *FEBS Lett.* 2002;526:135–141.
41. Garcia-Ruiz C, Colell A, Morales A, Calvo M, Enrich C, Fernandez-Checa JC. Trafficking of ganglioside GD3 to mitochondria by tumor necrosis factor-α. *J Biol Chem.* 2002;277: 36443–36448.

Drug Metab. Pharmacokinet. 28 (2): 118–124 (2013).

Regular Article

Comparison of Pharmacokinetics between Loxoprofen and Its Derivative with Lower Ulcerogenic Activity, Fluoro-loxoprofen

Naoki YAMAKAWA[1,2], Shintaro SUEMASU[1,2], Hiroshi WATANABE[2], Kayoko TAHARA[1], Ken-ichiro TANAKA[2], Yoshinari OKAMOTO[2], Masami OHTSUKA[2], Toru MARUYAMA[2] and Tohru MIZUSHIMA[1,2,*]

[1]*Department of Analytical Chemistry, Faculty of Pharmacy, Keio University, Tokyo, Japan*
[2]*Faculty of Life Sciences, Kumamoto University, Kumamoto, Japan*

Full text of this paper is available at http://www.jstage.jst.go.jp/browse/dmpk

Summary: We recently reported that, compared to loxoprofen (LOX, an non-steroidal anti-inflammatory drug), the LOX derivative fluoro-loxoprofen (F-LOX) is less ulcerogenic but has similar anti-inflammatory activity. Our previous *in vitro* studies suggested that both LOX and F-LOX are pro-drugs, the active metabolites of which are their *trans*-alcohol forms. In this study, we compared the pharmacokinetics of F-LOX and LOX in rats. Overall, the pharmacokinetic characteristics of F-LOX, including the formation of metabolites *in vivo* and *in vitro*, were comparable to those of LOX. However, F-LOX disappeared from the plasma more rapidly than LOX, which could potentially explain its lower ulcerogenicity. However, we showed that F-LOX produced fewer gastric lesions than LOX, even when a higher plasma concentration of F-LOX was maintained. Similar to LOX, F-LOX was readily metabolized to its *trans*- and *cis*-alcohol forms, with a higher level of the *trans*-alcohol form being observed after oral or intravenous administration of the drug. The preferential formation of the *trans*-alcohol form was also observed after incubation of F-LOX with rat liver homogenates *in vitro*. These results suggest that, similar to LOX, F-LOX acts as a pro-drug and that there is a metabolic system that selectively produces its active metabolite.

Keywords: loxoprofen; pharmacokinetics; liver homogenates; gastric lesions; rat

Introduction

Non-steroidal anti-inflammatory drugs (NSAIDs) comprise a useful family of therapeutics,[1] the actions of which are mediated *via* an inhibitory effect on cyclooxygenase (COX), an enzyme which is essential for the synthesis of inflammatory prostaglandins (PGs). However, NSAID use is also associated with gastrointestinal complications.[2–4] Given that PGs have a strong protective effect on the gastric mucosa, it was believed that NSAIDs induce gastric lesions only through the inhibition of COX. However, the increased incidence of gastrointestinal lesions and the decrease in PG levels induced by NSAIDs do not always occur in parallel,[5,6] suggesting that the former effect involves additional mechanisms. We have recently demonstrated that NSAIDs induce cell death in cultured gastric mucosal cells and at the gastric mucosa in a manner independent of COX inhibition but dependent on their membrane permeabilizing activity.[7–13] Furthermore, we suggested that both COX inhibition and gastric mucosal cell death are required for the formation of NSAID-induced gastric lesions.[11,14]

COX-1 and COX-2 are responsible for the majority of COX activity at the gastric mucosa and in tissues undergoing inflammation, respectively,[15,16] and a greatly reduced incidence of gastroduodenal lesions has been reported following treatment with selective COX-2 inhibitors (such as celecoxib and rofecoxib).[17,18] However, a recently raised concern regarding the use of selective COX-2 inhibitors involves the associated risk of cardiovascular thrombotic events.[19] This may be due to the fact that prostacyclin, a potent anti-aggregator of platelets and a vasodilator, is mainly produced by COX-2. Therefore, NSAIDs exhibiting gastrointestinal safety, other than selective COX-2 inhibitors, need to be developed. Based on our findings, we proposed that NSAIDs with lower membrane permeabilization activity would be easy on the stomach even in the absence of COX-2 selectivity.[9]

We screened for such NSAIDs from those used clinically and found that loxoprofen (LOX, **Fig. 1**) has lower membrane permeabilization activity and cytotoxicity than other NSAIDs.[20] LOX has been widely used in the Japanese market, because clinical studies have suggested that it is safer than other traditional NSAIDs,

Received May 24, 2012; Accepted July 31, 2012
J-STAGE Advance Published Date: August 14, 2012, doi:10.2133/dmpk.DMPK-12-RG-050
**To whom correspondence should be addressed:* Tohru MIZUSHIMA, Ph.D., *Department of Analytical Chemistry, Faculty of Pharmacy, Keio University, 1-5-30, Shibakoen, Minato-ku, Tokyo 105-8512, Japan. Tel. +81-3-5400-2628, Fax. +81-3-5400-2628, E-mail: mizushima-th@pha.keio.ac.jp*
This work was supported by Grants-in-Aid for Scientific Research from the Ministry of Health, Labour and Welfare of Japan, Grants-in-Aid for Scientific Research from the Ministry of Education, Culture, Sports, Science and Technology of Japan, and Grants-in-Aid from the Japan Science and Technology Agency.

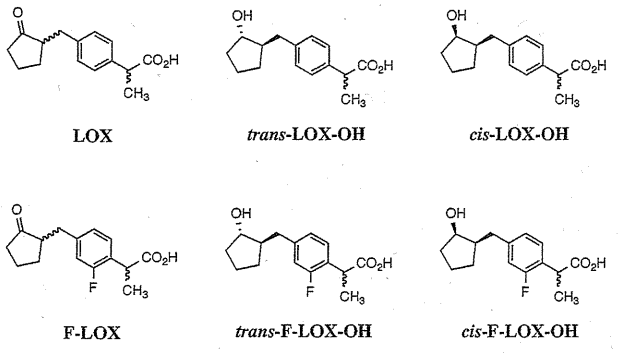

Fig. 1. Chemical structures of LOX, *trans*-LOX-OH, *cis*-LOX-OH, F-LOX, *trans*-F-LOX-OH and *cis*-F-LOX-OH

such as indomethacin.[21,22] LOX is a pro-drug, which is converted (by reduction of the cyclopentanone moiety) to its active *trans*-alcohol metabolite (*trans*-LOX-OH, **Fig. 1**) by multiple aldehyde-ketone reductases and carbonyl reductases only after absorption by the gastrointestinal tract.[23,24] We synthesized a series of LOX derivatives[25] and found that fluoro-loxoprofen (F-LOX, **Fig. 1**) has much lower membrane permeabilization and ulcerogenic activities than LOX but maintains similar anti-inflammatory activity.[26] We also suggested that the pro-drug property of LOX is maintained in F-LOX, based on the demonstration that the inhibitory activity of *trans*-F-LOX-OH (**Fig. 1**) on COX is more potent than that of F-LOX and its *cis*-alcohol metabolite (*cis*-F-LOX-OH, **Fig. 1**).[26] In this study, we compared the pharmacokinetics of LOX and F-LOX after oral or intravenous administration. Although some differences were observed, such as the more efficient absorption of F-LOX after its oral administration and its more rapid clearance from the plasma, the pharmacokinetic characters of F-LOX were basically comparable to those of LOX, including preferential metabolic formation of *trans*-F-LOX-OH rather than *cis*-F-LOX-OH. We therefore consider that F-LOX is likely to be a therapeutically beneficial NSAID due to its reduced gastric side effect.

Methods

Chemicals and animals: The sodium salts of LOX and F-LOX and their alcohol metabolites (*trans*-LOX-OH, *cis*-LOX-OH, *trans*-F-LOX-OH and *cis*-F-LOX-OH) were synthesized as reported previously[26] and their identities were confirmed by ^{1}H-NMR, ^{13}C-NMR, FAB-MS spectrum and elemental analysis (within ± 0.4% of the theoretical values). The purity of each tested compound was greater than 95% as assessed by high performance liquid chromatography (HPLC).

HPLC-grade acetonitrile was purchased from Sigma-Aldrich (St. Louis, MO). Wistar rats (6 weeks old, 180–200 g, male) were obtained from Kyudo Co. (Kumamoto, Japan). The experiments and procedures described here were carried out in accordance with the Guide for the Care and Use of Laboratory Animals as adopted and promulgated by the National Institutes of Health (Bethesda, MD), and were approved by the Animal Care Committee of Keio University and Kumamoto University.

HPLC analysis: The analytical HPLC with reverse-phase column (TSKgel Super-ODS, 150 × 4.6 mm, 2 µm, Tosoh Co., Tokyo, Japan) incorporated a Waters 2695 Alliance separation module and a Waters 2996 photodiode array detector (Waters, Milford, MA). Solvent A (0.1% trifluoroacetic acid in acetonitrile) and solvent B (0.1% trifluoroacetic acid in water) were used at a flow rate of 0.3 ml/min. After injection of the sample (0 min), the mobile phase was changed as follows: 35% solvent A (10 min), a linear gradient of 35–100% solvent A (3 min) and 100% solvent A (3 min). Detection was performed at an optical density of 220 nm.

Drug administration and pharmacokinetic analysis: Each compound was dissolved in saline and administered to rats at a dose of 20 mg/kg, orally or intravenously (*via* the tail vein). Tail vein blood samples (200 µl) were taken periodically (15, 30, 45, 60, 120 and 240 min after drug administration) into centrifuge tubes containing heparin. Samples were centrifuged immediately to obtain plasma. An aliquot (100 µl) of plasma was mixed with 500 µl of methanol to extract each compound and its metabolites. The suspension was centrifuged and the supernatant was analyzed by HPLC as described above.

Pharmacokinetic data analysis: A non-compartment model was used for the pharmacokinetic analysis. Each parameter, time of maximum concentration (T_{max}, min), maximum concentration (C_{max}, µg/ml), apparent elimination half-life ($t_{1/2}$, min), area under the concentration-time curve from time 0 to infinite times ($AUC_{0-\infty}$, µg/ml/min), mean residence time from time 0 to infinite times ($MRT_{0-\infty}$, min), total plasma clearance (CL_{tot}, ml/min/kg) and volume of distribution at the steady state (Vd_{ss}, ml), was calculated using the moment analysis program available on Microsoft Excel. The absolute oral bioavailability (F, %) was calculated using the following equation:

$$F(\%) = \frac{\text{Mean } AUC_{0-\infty,p.o.} \times \text{Dose}_{i.v.}}{\text{Mean } AUC_{0-\infty,i.v.} \times \text{Dose}_{p.o.}} \times 100$$

Drug treatment of rat liver homogenates *in vitro*: *In vitro* analysis for metabolic conversion of F-LOX and LOX was performed as described previously,[27] with some modifications. Rat livers were homogenized with PBS (1 ml PBS/g tissue) using a tissue homogenizer (Silent Crusher M, Heidolph, Germany). Each test compound in PBS (100 µl, 5 mg/ml) was mixed with 2 ml of the homogenates and incubated for various periods (10, 20, 30, 60, 120 and 240 min) at 37°C. The reaction was terminated by addition of 1.8 ml of methanol and the solution was centrifuged. The supernatant was analyzed by HPLC as described above.

Gastric damage assay: The gastric ulcerogenic response was examined as described previously,[25,28] with some modifications. Rats fasted for 18 h were orally administered LOX or F-LOX and, after 8 h, the animals were sacrificed, their stomachs were removed, and the areas of gastric mucosal lesions were measured by an observer unaware of the treatment that the animals had received. Calculation of the scores involved measuring the area of all the lesions in square millimeters and summing the values to give an overall lesion index.

Statistical analysis: All values are expressed as the mean ± S.D. or mean ± S.E.M. One-way or two-way analysis of variance (ANOVA) followed by the Tukey's test was used to evaluate differences among more than three groups. The Student's *t*-test for unpaired results was used for the evaluation of differences between two groups. Differences were considered to be significant for values of $p < 0.05$.

Results and Discussion

Pharmacokinetic analysis after oral or intravenous administration of LOX or F-LOX: We first compared the temporal profile of the plasma concentration following oral administration of

LOX and F-LOX (**Figs. 2A** and **2B**) and calculated the pharmacokinetic parameters based on moment analysis (non-compartment model) (**Table 1**). The pharmacokinetic characteristics of LOX (**Fig. 2**) were basically similar to those described previously,[27] and in general, the pharmacokinetic characteristics of F-LOX were comparable to those of LOX, as described below.

The C_{max} of F-LOX was significantly higher than that of LOX (**Table 1**), suggesting that F-LOX was absorbed more rapidly at the gastrointestinal mucosa. However, F and T_{max} values were not different between both F-LOX and LOX (**Table 1**). This may be due to the fact that the clearance of F-LOX is faster than LOX (see below).

The plasma level of F-LOX following oral administration (at 2 or 4 h) was lower than that of LOX (**Figs. 2A** and **2B**) and the $MRT_{0-\infty}$ and $t_{1/2}$ of the former drug were shorter (**Table 1**). We concluded that F-LOX was cleared from the plasma more rapidly than LOX. The $AUC_{0-\infty}$ of F-LOX following oral administration was smaller than that of LOX (**Table 1**).

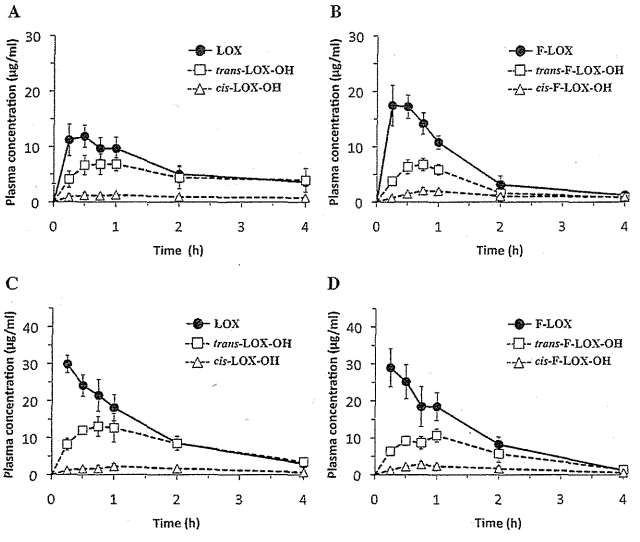

Fig. 2. Plasma concentrations of LOX and F-LOX and their metabolites following their oral or intravenous administration
Rats were administered LOX (A, C) or F-LOX (B, D) orally (A, B) or intravenously (C, D). The plasma concentration of each form of the drugs was monitored as described in Methods. Values are mean ± S.D. ($n = 4$–6).

We also monitored the temporal profile of the plasma concentrations of metabolites of LOX or F-LOX (*trans*-LOX-OH and *cis*-LOX-OH or *trans*-F-LOX-OH and *cis*-F-LOX-OH) after their oral administration and found that, similar to LOX, F-LOX was readily metabolized (**Figs. 2A** and **2B**). As previously described,[24,27,29] a relatively higher plasma level of *trans*-LOX-OH than *cis*-LOX-OH was observed (**Fig. 2A**). Similar results were observed for F-LOX (**Fig. 2B**). It is well known that LOX is metabolized to *trans*- or *cis*-LOX-OH with a stereoselectivity and multiple enzymes are involved in this stereoselectivity in humans.[24,30] Results in this study suggest that the system for this stereoselective reduction is common between rats and humans, which was suggested by the previous paper.[31,32] The C_{max} of *trans*-F-LOX-OH (active metabolite) after oral administration of F-LOX was similar to that of LOX (**Table 1**). However, the $t_{1/2}$ and and $AUC_{0-\infty}$ of *trans*-F-LOX-OH were shorter and smaller, respectively, than those of LOX (**Table 1**). We also calculated each pharmacokinetic parameter of *cis*-LOX-OH and *cis*-F-LOX-OH (**Table 1**); however, as the plasma level of each *cis*-OH form was very low, the accuracy of these results is debatable.

We also compared the plasma concentration-time profiles of LOX and F-LOX following their intravenous administration (**Figs. 2C** and **2D**). As in the case of oral administration, the $MRT_{0-\infty}$ and $t_{1/2}$ of F-LOX were shorter than those of LOX (**Table 1**), confirming the more rapid plasma clearance of the former drug. Compared to LOX, CL_{tot} of F-LOX after its intravenous administration tended to be higher, although this difference was not statistically significant (**Table 1**). The preferential conversion of F-LOX or LOX to its *trans*-OH rather than *cis*-OH form was also confirmed following intravenous administration (**Figs. 2C** and **2D**).

Pharmacokinetic analysis after administration of the *trans*- and *cis*-OH forms of LOX and F-LOX: We next compared the plasma concentration-time profile of each form of LOX and F-LOX after oral or intravenous administration of the *trans*- or

Table 1. Pharmacokinetic parameters after oral (*p.o.*, upper) or intravenous (i.v., lower) administration of LOX or F-LOX

Pharmacokinetic parameters	Unit	LOX *p.o.* (20.0 mg/kg)			F-LOX *p.o.* (21.3 mg/kg)		
		LOX	*trans*-LOX-OH	*cis*-LOX-OH	F-LOX	*trans*-F-LOX-OH	*cis*-F-LOX-OH
T_{max}	min	20 ± 9	45 ± 15	50 ± 17	20 ± 8.7	45 ± 0	70 ± 43
C_{max}	μg/ml	13.7 ± 1.9	8.3 ± 0.5	1.5 ± 0.2	19.5 ± 1.4*	6.5 ± 1.2	2.4 ± 0.3*
$t_{1/2}$	min	127 ± 32	373 ± 149	332 ± 100	59 ± 11*	105 ± 20*	132 ± 34*
$AUC_{0-\infty}$	μg/ml·min	2,419 ± 390	4,133 ± 1,908	827 ± 456	1,689 ± 186*	1,032 ± 34*	611 ± 184
$MRT_{0-\infty}$	min	192 ± 45	548 ± 217	577 ± 278	94 ± 19*	167 ± 28*	240 ± 47
F	%	61	—	—	51	—	—

Pharmacokinetic parameters	Unit	LOX i.v. (20.0 mg/kg)			F-LOX i.v. (21.3 mg/kg)		
		LOX	*trans*-LOX-OH	*cis*-LOX-OH	F-LOX	*trans*-F-LOX-OH	*cis*-F-LOX-OH
T_{max}	min	—	38 ± 8	49 ± 6	—	60 ± 0	75 ± 26
C_{max}	μg/ml	—	13.5 ± 2	2.4 ± 0.6	—	10.7 ± 1.5	3.5 ± 0.3*
$t_{1/2}$	min	68 ± 5	109 ± 19	114 ± 20	48 ± 6*	85 ± 5	71 ± 3*
$AUC_{0-\infty}$	μg/ml·min	3,227 ± 336	2,412 ± 172	445 ± 45	2,775 ± 324	1,502 ± 346**	487 ± 65
$MRT_{0-\infty}$	min	98 ± 8	173 ± 24	186 ± 24	72 ± 8**	134 ± 4*	129 ± 7**
CL_{tot}	ml/min/kg	6.3 ± 0.7	—	—	7.3 ± 0.9	—	—
Vd_{ss}	ml	609 ± 49	—	—	530 ± 108	—	—

Data in **Figure 2** were used to calculate each pharmacokinetic parameter as described in Methods. Values are mean ± S.D. ($n = 4$–6). *$p < 0.05$, **$p < 0.01$ (*vs.* LOX and its metabolites).

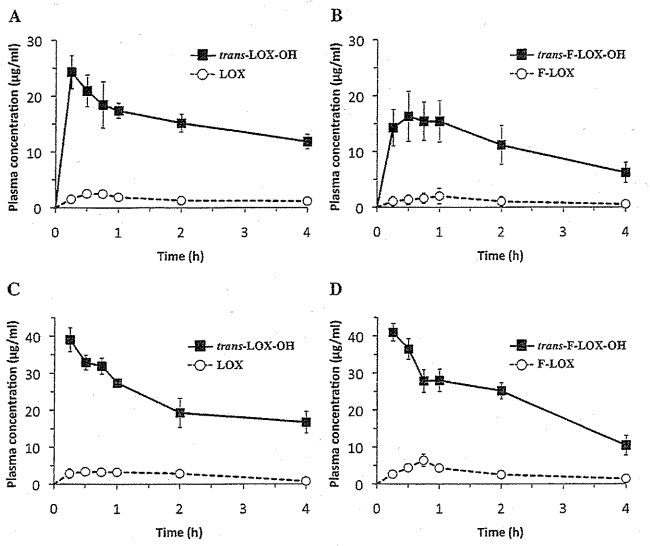

Fig. 3. Plasma concentration of *trans*-LOX-OH and *trans*-F-LOX-OH and their metabolites following their oral or intravenous administration
Rats were administered *trans*-LOX-OH (A, C) or *trans*-F-LOX-OH (B, D) orally (A, B) or intravenously (C, D). The plasma concentration of each form of the drugs was monitored. Values are mean ± S.D. ($n = 4$–6).

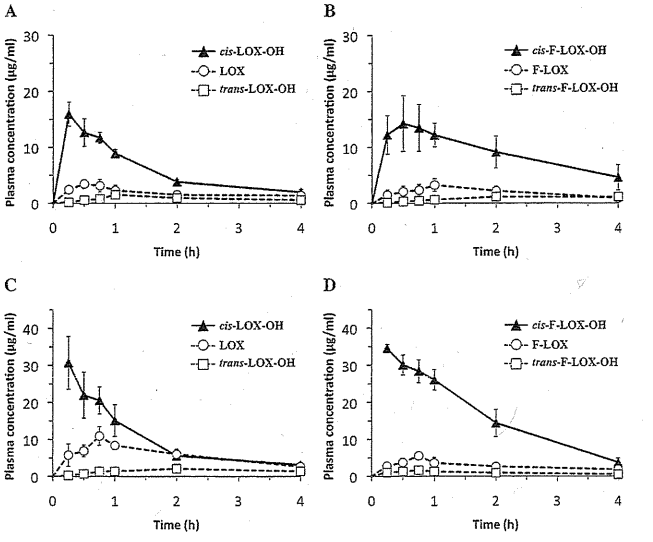

Fig. 4. Plasma concentration of *cis*-LOX-OH and *cis*-F-LOX-OH and their metabolites following their oral or intravenous administration
Rats were administered *cis*-LOX-OH (A, C) or *cis*-F-LOX-OH (B, D) orally (A, B) or intravenously (C, D). The plasma concentration of each form of the drugs was monitored. Values are mean ± S.D. ($n = 4$–6).

Table 2. Pharmacokinetic parameters after oral (*p.o.*, upper) or intravenous (i.v., lower) administration of the *trans*-OH form of LOX or F-LOX

Pharmacokinetic parameters	Unit	*trans*-LOX-OH *p.o.* (20.0 mg/kg)			*trans*-F-LOX-OH *p.o.* (21.3 mg/kg)		
		trans-LOX-OH	LOX	*cis*-LOX-OH	*trans*-F-LOX-OH	F-LOX	*cis*-F-LOX-OH
T_{max}	min	15 ± 0	35 ± 7	N.D.	38 ± 13	60 ± 0	N.D.
C_{max}	μg/ml	25.0 ± 3	2.9 ± 0.4	N.D.	16.5 ± 3.7*	2.0 ± 1.2	N.D.
$t_{1/2}$	min	227 ± 28	149 ± 8	N.D.	145 ± 20*	91 ± 52	N.D.
$AUC_{0-\infty}$	μg/ml·min	7,229 ± 762	558 ± 165	N.D.	3,889 ± 964**	360 ± 276	N.D.
$MRT_{0-\infty}$	min	336 ± 39	233 ± 13	N.D.	216 ± 25**	154 ± 74	N.D.
F	%	81	—	—	60	—	—

Pharmacokinetic parameters	Unit	*trans*-LOX-OH i.v. (20.0 mg/kg)			*trans*-F-LOX-OH i.v. (21.3 mg/kg)		
		trans-LOX-OH	LOX	*cis*-LOX-OH	*trans*-F-LOX-OH	F-LOX	*cis*-F-LOX-OH
T_{max}	min	—	53 ± 40	N.D.	—	45 ± 0	N.D.
C_{max}	μg/ml	—	4.2 ± 0.5	N.D.	—	6.4 ± 1.4*	N.D.
$t_{1/2}$	min	193 ± 36	75 ± 16	N.D.	129 ± 27*	100 ± 21	N.D.
$AUC_{0-\infty}$	μg/ml·min	9,920 ± 1,809	538 ± 93	N.D.	7,611 ± 999	662 ± 103	N.D.
$MRT_{0-\infty}$	min	282 ± 52	99 ± 12	N.D.	174 ± 25*	99 ± 8	N.D.
CL_{tot}	ml/min/kg	2.1 ± 0.4	—	—	2.7 ± 0.4	—	—
Vd_{ss}	ml	570 ± 42	—	—	456 ± 10**	—	—

Data in **Figure 3** were used to calculate each pharmacokinetic parameter as described in Methods. Values are mean ± S.D. ($n = 4$–6). *$p < 0.05$, **$p < 0.01$ (*vs.* LOX and its metabolites). N.D., not detected.

cis-OH form. As shown in **Figures 3** and **4**, LOX was detected after oral or intravenous administration of *trans*-LOX-OH or *cis*-LOX-OH. *trans*-LOX-OH was detected after oral or intravenous administration of *cis*-LOX-OH; however, *cis*-LOX-OH was not detected after oral or intravenous administration of *trans*-LOX-OH (**Figs. 3** and **4**). These results are consistent with those reported previously.[33] Similar results were also observed for F-LOX (**Figs. 3** and **4**), suggesting that there is a metabolic system which converts *trans*- or *cis*-F-LOX-OH to F-LOX. Our results also support the idea that the metabolic system converts F-LOX preferentially to *trans*-F-LOX-OH rather than to *cis*-F-LOX-OH, the assumption being that *trans*-F-LOX-OH is produced from *cis*-F-LOX-OH *via* F-LOX.

The data in **Table 2** show that the C_{max} of *trans*-F-LOX-OH was less than that of *trans*-LOX-OH following their oral administration, suggesting that the absorption of *trans*-F-LOX-OH was slower, in contrast to the situation with the ketone forms of these NSAIDs (**Table 1**). However, the $t_{1/2}$ and $MRT_{0-\infty}$ of *trans*-F-LOX-OH were shorter than those of *trans*-LOX-OH following both oral and intravenous administration (**Table 2**), this being consistent with what is observed in the case of their ketone forms (**Table 1**).

The data in **Table 3** show that the pharmacokinetic characteristics of *cis*-F-LOX-OH, relative to *cis*-LOX-OH, differed from those of F-LOX and *trans*-F-LOX-OH. For example, the $MRT_{0-\infty}$ of *cis*-F-LOX-OH was longer than that of *cis*-LOX-OH after oral administration and $AUC_{0-\infty}$ or CL_{tot} of *cis*-F-LOX-OH was higher or lower than that of *cis*-LOX-OH after intravenous administration (**Table 3**). However, as the *cis*-OH forms of F-LOX and LOX are inactive in terms of COX-inhibition,[26] these results may not be clinically or pharmacologically relevant.

Table 3. Pharmacokinetic parameters after oral (*p.o.*, upper) or intravenous (i.v., lower) administration of the *cis*-OH form of LOX or F-LOX

Pharmacokinetic parameters	Unit	*cis*-LOX-OH *p.o.* (20.0 mg/kg)			*cis*-F-LOX-OH *p.o.* (21.3 mg/kg)		
		cis-LOX-OH	LOX	*trans*-LOX-OH	*cis*-F-LOX-OH	F-LOX	*trans*-F-LOX-OH
T_{max}	min	15 ± 0	34 ± 6	60 ± 0	38 ± 13	56 ± 6	60 ± 0
C_{max}	μg/ml	15.2 ± 1.5	3.4 ± 0.7	1.5 ± 0.4	14.6 ± 3.8	3.4 ± 0.9	1.4 ± 0.4
$t_{1/2}$	min	74 ± 9	200 ± 53	143 ± 37	123 ± 34	93 ± 30*	93 ± 10.2
$AUC_{0-\infty}$	μg/ml·min	1,557 ± 85	926 ± 314	317 ± 97	3,037 ± 1,076	593 ± 260	372 ± 157
$MRT_{0-\infty}$	min	113 ± 13	383 ± 158	247 ± 53	191 ± 46*	165 ± 38	236 ± 50
F	%	59	—	—	75	—	—

Pharmacokinetic parameters	Unit	*cis*-LOX-OH i.v. (20.0 mg/kg)			*cis*-F-LOX-OH i.v. (21.3 mg/kg)		
		cis-LOX-OH	LOX	*trans*-LOX-OH	*cis*-F-LOX-OH	F-LOX	*trans*-F-LOX-OH
T_{max}	min	—	49 ± 6	101 ± 32	—	45 ± 0	45 ± 0
C_{max}	μg/ml	—	11.2 ± 1.7	2.4 ± 0.5	—	5.6 ± 0.9*	1.7 ± 0.3
$t_{1/2}$	min	68 ± 1	98 ± 7	175 ± 89	69 ± 8	111 ± 31	176 ± 53
$AUC_{0-\infty}$	μg/ml·min	2,785 ± 429	1,707 ± 70	757 ± 402	4,387 ± 602*	932 ± 183**	442 ± 124
$MRT_{0-\infty}$	min	94 ± 2	164 ± 7	312 ± 123	100 ± 11	189 ± 43	334 ± 115
CL_{tot}	ml/min/kg	7.4 ± 1.3	—	—	4.6 ± 0.6*	—	—
Vd_{ss}	ml	697 ± 138	—	—	460 ± 27*	—	—

Data in **Figure 4** were used to calculate each pharmacokinetic parameter as described in Methods. Values are mean ± S.D. ($n = 4$–6). *$p < 0.05$, **$p < 0.01$ (*vs.* LOX and its metabolites).

Metabolic conversion of F-LOX and LOX *in vitro*: It has previously been reported that LOX is metabolized in the liver *in vivo* and that the conversion of LOX to *trans*- or *cis*-LOX-OH can be reproduced *in vitro* using rat liver homogenates.[34] Using this system, we examined the conversion of F-LOX to its *trans*- or *cis*-OH form *in vitro*. We first showed that incubation of LOX with rat liver homogenates produced a higher level of *trans*-LOX-OH than *cis*-LOX-OH (**Fig. 5A**). Although both *trans*-LOX-OH and *cis*-LOX-OH were more stable than LOX in this system, incubation of *trans*-LOX-OH or *cis*-LOX-OH with the homogenates generated only LOX or both LOX and *trans*-LOX-OH, respectively (**Figs. 5A–5C**). These results are consistent with those previously reported.[34] As shown in **Figures 5D–5F**, results obtained with F-LOX were essentially similar to those seen with LOX. Incubation of F-LOX with rat liver homogenates produced a higher level of *trans*-F-LOX-OH than *cis*-F-LOX-OH (**Fig. 5D**). Given that the formation of *trans*- or *cis*-F-LOX-OH was associated with concomitant loss of F-LOX and the sum of F-LOX, *trans*-F-LOX-OH and *cis*-F-LOX-OH was consistent throughout the incubation (**Fig. 5D**), it appears that the homogenates metabolized F-LOX selectively to *trans*-F-LOX-OH and *cis*-F-LOX-OH. Incubation of *trans*-F-LOX-OH or *cis*-F-LOX-OH with the homogenates generated F-LOX and the conversion from *trans*-F-LOX-OH was more efficient that from *cis*-F-LOX-OH (**Figs. 5E** and **5F**). Furthermore, although the incubation of *cis*-F-LOX-OH with the homogenates generated *trans*-F-LOX-OH, the opposite did not occur (**Figs. 5E** and **5F**). These results correlate well with the *in vivo* findings illustrated in **Figures 3** and **4**. The results in **Figure 5** suggest that there is a metabolic system that converts F-LOX and LOX preferentially to their *trans*-OH rather than *cis*-OH forms.

Results in **Figure 5** show that the disappearance rate of F-LOX was similar to that of LOX. Therefore, the more rapid clearance of F-LOX than LOX that was observed *in vivo* could not be explained by its metabolic conversion in the liver. The examination of the urinary clearance and protein binding would be required to understand the mechanism for the difference in pharmacokinetics between the two drugs.

Production of gastric lesions by F-LOX and LOX: We have previously reported that F-LOX produces fewer gastric lesions than

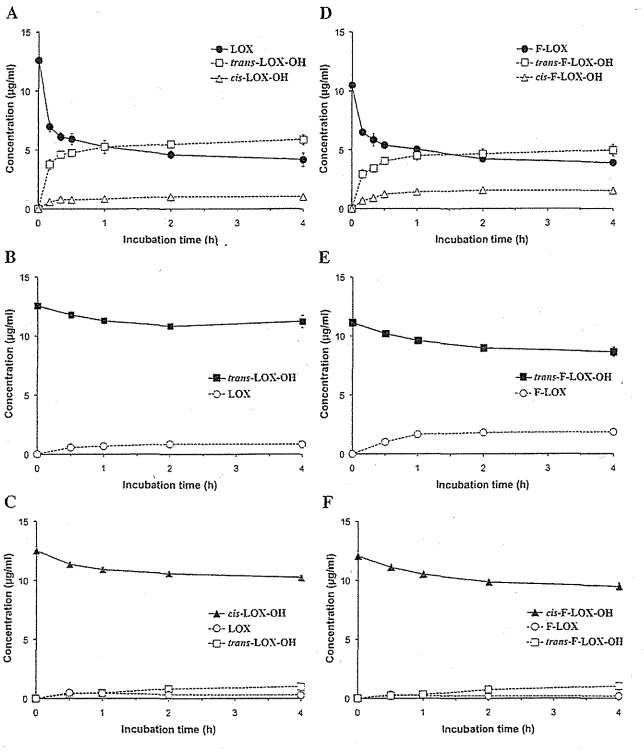

Fig. 5. Metabolic conversion of LOX and F-LOX and their metabolites in rat liver homogenates *in vitro*
Each drug [LOX (A), *trans*-LOX-OH (B), *cis*-LOX-OH (C), F-LOX (D), *trans*-F-LOX-OH (E) and *cis*-F-LOX-OH (F)] (500 μg) was incubated with rat liver homogenates at 37°C. Samples were obtained periodically and the amount of each form of LOX or F-LOX was determined. Values are mean ± S.E.M. ($n = 3$).

LOX in rats, and proposed that this lower ulcerogenic activity of F-LOX is due to its lower membrane permeabilization activity.[26] However, given that the results demonstrate that F-LOX and its active metabolite (*trans*-F-LOX-OH) disappear from the plasma more rapidly than LOX, it is also possible that the lower ulcerogenic activity of F-LOX is due to its lower plasma level after a

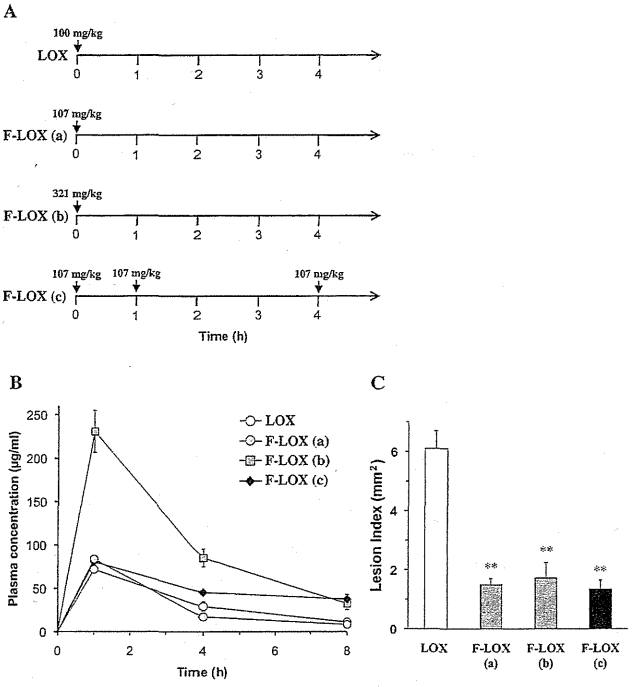

Fig. 6. Production of gastric lesions by LOX or F-LOX
The administration protocols for LOX or F-LOX are shown (A): rats were orally administered 100 mg/kg of LOX once only at time 0, 107 mg/kg of F-LOX once only at time 0 (a), 321 mg/kg of F-LOX once only at time 0 (b), or 107 mg/kg of F-LOX at 0, 1 and 4 h (c). The plasma concentration of LOX or F-LOX was monitored (B). Stomachs were removed after 8 h and scored for hemorrhagic damage (C). Values are mean ± S.E.M. ($n = 4$). $^{**}p < 0.01$ (*vs.* LOX).

single oral administration. To test this possibility, we performed the experiments illustrated in **Figure 6**. In this study, in order to keep the plasma concentration of F-LOX higher than that of LOX, rats were either administered a 3-fold higher dose of F-LOX than LOX or administered the same dose of F-LOX as LOX but at 3 time-points (0, 1 and 4 h) (**Fig. 6A**). As shown in **Figure 6B**, a consistently higher plasma concentration of F-LOX than LOX was achieved using these protocols. Administration of F-LOX produced fewer gastric lesions than LOX in all cases (**Fig. 6C**), strongly suggesting that the lower ulcerogenic activity of the former drug cannot be explained by the differences in its pharmacokinetic characteristics. In other words, the lower ulcerogenic activity of F-LOX seems to be derived from other properties, such as its lower membrane permeabilization activity.

Conclusions: In this study, we compared the pharmacokinetics of F-LOX and LOX. Although some differences were observed, it should be noted that the pharmacokinetic characteristics of F-LOX are basically comparable to those of LOX. In particular, it is important to note that the metabolic conversion characteristics of the ketone, *trans*-OH- and *cis*-OH forms of LOX were maintained in F-LOX, given that the pro-drug properties of LOX are believed to play important roles in its clinically beneficial effects, including its potent anti-inflammatory action and low gastrointestinal side effect. Therefore, the results in this study confirm the idea that F-LOX is a LOX analog with reduced gastrointestinal side effects and suggest that it is likely to be a therapeutically safer NSAID.

References

1) Smalley, W. E., Ray, W. A., Daugherty, J. R. and Griffin, M. R.: Nonsteroidal anti-inflammatory drugs and the incidence of hospitalizations for peptic ulcer disease in elderly persons. *Am. J. Epidemiol.*, **141**: 539–545 (1995).
2) Hawkey, C. J.: Nonsteroidal anti-inflammatory drug gastropathy. *Gastroenterology*, **119**: 521–535 (2000).
3) Barrier, C. H. and Hirschowitz, B. I.: Controversies in the detection and management of nonsteroidal antiinflammatory drug-induced side effects of the upper gastrointestinal tract. *Arthritis Rheum.*, **32**: 926–932 (1989).
4) Fries, J. F., Miller, S. R., Spitz, P. W., Williams, C. A., Hubert, H. B. and Bloch, D. A.: Toward an epidemiology of gastropathy associated with nonsteroidal antiinflammatory drug use. *Gastroenterology*, **96**: 647–655 (1989).
5) Ligumsky, M., Golanska, E. M., Hansen, D. G. and Kauffman, G. J.: Aspirin can inhibit gastric mucosal cyclo-oxygenase without causing lesions in rat. *Gastroenterology*, **84**: 756–761 (1983).
6) Ligumsky, M., Sestieri, M., Karmeli, F., Zimmerman, J., Okon, E. and Rachmilewitz, D.: Rectal administration of nonsteroidal antiinflammatory drugs. Effect on rat gastric ulcerogenicity and prostaglandin E2 synthesis. *Gastroenterology*, **98**: 1245–1249 (1990).
7) Tanaka, K., Tomisato, W., Hoshino, T., Ishihara, T., Namba, T., Aburaya, M., Katsu, T., Suzuki, K., Tsutsumi, S. and Mizushima, T.: Involvement of intracellular Ca^{2+} levels in nonsteroidal anti-inflammatory drug-induced apoptosis. *J. Biol. Chem.*, **280**: 31059–31067 (2005).
8) Tsutsumi, S., Gotoh, T., Tomisato, W., Mima, S., Hoshino, T., Hwang, H. J., Takenaka, H., Tsuchiya, T., Mori, M. and Mizushima, T.: Endoplasmic reticulum stress response is involved in nonsteroidal anti-inflammatory drug-induced apoptosis. *Cell Death Differ.*, **11**: 1009–1016 (2004).
9) Tomisato, W., Tanaka, K., Katsu, T., Kakuta, H., Sasaki, K., Tsutsumi, S., Hoshino, T., Aburaya, M., Li, D., Tsuchiya, T., Suzuki, K., Yokomizo, K. and Mizushima, T.: Membrane permeabilization by non-steroidal anti-inflammatory drugs. *Biochem. Biophys. Res. Commun.*, **323**: 1032–1039 (2004).
10) Tomisato, W., Tsutsumi, S., Rokutan, K., Tsuchiya, T. and Mizushima, T.: NSAIDs induce both necrosis and apoptosis in guinea pig gastric mucosal cells in primary culture. *Am. J. Physiol. Gastrointest. Liver Physiol.*, **281**: G1092–G1100 (2001).
11) Aburaya, M., Tanaka, K., Hoshino, T., Tsutsumi, S., Suzuki, K., Makise, M., Akagi, R. and Mizushima, T.: Heme oxygenase-1 protects gastric mucosal cells against non-steroidal anti-inflammatory drugs. *J. Biol. Chem.*, **281**: 33422–33432 (2006).
12) Tsutsumi, S., Namba, T., Tanaka, K. I., Arai, Y., Ishihara, T., Aburaya, M., Mima, S., Hoshino, T. and Mizushima, T.: Celecoxib upregulates endoplasmic reticulum chaperones that inhibit celecoxib-induced apoptosis in human gastric cells. *Oncogene*, **25**: 1018–1029 (2006).
13) Namba, T., Hoshino, T., Tanaka, K., Tsutsumi, S., Ishihara, T., Mima, S., Suzuki, K., Ogawa, S. and Mizushima, T.: Up-regulation of 150-kDa oxygen-regulated protein by celecoxib in human gastric carcinoma cells. *Mol. Pharmacol.*, **71**: 860–870 (2007).
14) Tomisato, W., Tsutsumi, S., Hoshino, T., Hwang, H. J., Mio, M., Tsuchiya, T. and Mizushima, T.: Role of direct cytotoxic effects of NSAIDs in the induction of gastric lesions. *Biochem. Pharmacol.*, **67**: 575–585 (2004).
15) Kujubu, D. A., Fletcher, B. S., Varnum, B. C., Lim, R. W. and Herschman, H. R.: TIS10, a phorbol ester tumor promoter-inducible mRNA from Swiss 3T3 cells, encodes a novel prostaglandin synthase/cyclooxygenase homologue. *J. Biol. Chem.*, **266**: 12866–12872 (1991).
16) Xie, W. L., Chipman, J. G., Robertson, D. L., Erikson, R. L. and Simmons, D. L.: Expression of a mitogen-responsive gene encoding prostaglandin synthase is regulated by mRNA splicing. *Proc. Natl. Acad. Sci. USA*, **88**: 2692–2696 (1991).
17) Silverstein, F. E., Faich, G., Goldstein, J. L., Simon, L. S., Pincus, T., Whelton, A., Makuch, R., Eisen, G., Agrawal, N. M., Stenson, W. F., Burr, A. M., Zhao, W. W., Kent, J. D., Lefkowith, J. B., Verburg, K. M. and Geis, G. S.: Gastrointestinal toxicity with celecoxib vs nonsteroidal anti-inflammatory drugs for osteoarthritis and rheumatoid arthritis: the CLASS study: A randomized controlled trial. Celecoxib Long-term Arthritis Safety Study. *JAMA*, **284**: 1247–1255 (2000).
18) Bombardier, C., Laine, L., Reicin, A., Shapiro, D., Burgos, V. R., Davis, B., Day, R., Ferraz, M. B., Hawkey, C. J., Hochberg, M. C., Kvien, T. K. and Schnitzer, T. J.: Comparison of upper gastrointestinal toxicity of rofecoxib and naproxen in patients with rheumatoid arthritis. VIGOR Study Group. *N. Engl. J. Med.*, **343**: 1520–1528 (2000).
19) Mukherjee, D., Nissen, S. E. and Topol, E. J.: Risk of cardiovascular

events associated with selective COX-2 inhibitors. *JAMA*, **286**: 954–959 (2001).
20) Yamakawa, N., Suemasu, S., Kimoto, A., Arai, Y., Ishihara, T., Yokomizo, K., Okamoto, Y., Otsuka, M., Tanaka, K. and Mizushima, T.: Low direct cytotoxicity of loxoprofen on gastric mucosal cells. *Biol. Pharm. Bull.*, **33**: 398–403 (2010).
21) Misaka, E., Yamaguchi, T., Iizuka, Y., Kamoshida, K., Kojima, T., Kobayashi, K., Endo, Y., Misawa, Y., Lobayashi, S. and Tanaka, K.: Anti-inflammatory, Analgesic and Antipyretic Activities of Sodium 2-[4-(2-oxocyclopentan-1-ylmethyl)phenyl] Propionate Dihydrate (CS-600). *Pharmacometrics*, **21**: 753–771 (1981).
22) Kawano, S., Tsuji, S., Hayashi, N., Takei, Y., Nagano, K., Fusamoto, H. and Kamada, T.: Effects of loxoprofen sodium, a newly synthesized non-steroidal anti-inflammatory drug, and indomethacin on gastric mucosal haemodynamics in the human. *J. Gastroenterol. Hepatol.*, **10**: 81–85 (1995).
23) Sugimoto, M., Kojima, T., Asami, M., Iizuka, Y. and Matsuda, K.: Inhibition of prostaglandin production in the inflammatory tissue by loxoprofen-Na, an anti-inflammatory prodrug. *Biochem. Pharmacol.*, **42**: 2363–2368 (1991).
24) Ohara, H., Miyabe, Y., Deyashiki, Y., Matsuura, K. and Hara, A.: Reduction of drug ketones by dihydrodiol dehydrogenases, carbonyl reductase and aldehyde reductase of human liver. *Biochem. Pharmacol.*, **50**: 221–227 (1995).
25) Yamakawa, N., Suemasu, S., Matoyama, M., Tanaka, K.-i., Katsu, T., Miyata, K., Okamoto, Y., Otsuka, M. and Mizushima, T.: Synthesis and biological evaluation of loxoprofen derivatives. *Bioorg. Med. Chem.*, **19**: 3299–3311 (2011).
26) Yamakawa, N., Suemasu, S., Matoyama, M., Kimoto, A., Takeda, M., Tanaka, K., Ishihara, T., Katsu, T., Okamoto, Y., Otsuka, M. and Mizushima, T.: Properties and synthesis of 2-{2-fluoro (or bromo)-4-[(2-oxocyclopentyl)methyl]phenyl}propanoic acid: nonsteroidal anti-inflammatory drugs with low membrane permeabilizing and gastric lesion-producing activities. *J. Med. Chem.*, **53**: 7879–7882 (2010).
27) Koo, T. S., Kim, D. H., Ahn, S. H., Kim, K. P., Kim, I. W., Seo, S. Y., Suh, Y. G., Kim, D. D., Shim, C. K. and Chung, S. J.: Comparison of pharmacokinetics of loxoprofen and its active metabolites after an intravenous, intramuscular, and oral administration of loxoprofen in rats: evidence for extrahepatic metabolism. *J. Pharm. Sci.*, **94**: 2187–2197 (2005).
28) Suemasu, S., Tanaka, K., Namba, T., Ishihara, T., Katsu, T., Fujimoto, M., Adachi, H., Sobue, G., Takeuchi, K., Nakai, A. and Mizushima, T.: A role for HSP70 in protecting against indomethacin-induced gastric lesions. *J. Biol. Chem.*, **284**: 19705–19715 (2009).
29) Choo, K. S., Kim, I. W., Jung, J. K., Suh, Y. G., Chung, S. J., Lee, M. H. and Shim, C. K.: Simultaneous determination of loxoprofen and its diastereomeric alcohol metabolites in human plasma and urine by a simple HPLC-UV detection method. *J. Pharm. Biomed. Anal.*, **25**: 639–650 (2001).
30) Naganuma, H., Mochizuki, Y. and Kawahara, Y.: Study of pharmacokinetics following oral administration of loxprofen sodium (CS-600) in humans. *J. Clin. Ther. Med.*, **2**: 1219–1237 (1986).
31) Pawlowski, J. E., Huizinga, M. and Penning, T. M.: Cloning and sequencing of the cDNA for rat liver 3 alpha-hydroxysteroid/dihydrodiol dehydrogenase. *J. Biol. Chem.*, **266**: 8820–8825 (1991).
32) Deyashiki, Y., Ogasawara, A., Nakayama, T., Nakanishi, M., Miyabe, Y., Sato, K. and Hara, A.: Molecular cloning of two human liver 3 alpha-hydroxysteroid/dihydrodiol dehydrogenase isoenzymes that are identical with chlordecone reductase and bile-acid binder. *Biochem. J.*, **299**(Pt 2): 545–552 (1994).
33) Tanaka, Y.: Stereoselective metabolism studies on loxoprofen, a 2-arylpropionic acid nonsteroidal anti-inflammatory drug, and its role for the development as a prodrug. *Drug Metab. Pharmacokinet.*, **8**: 521–536 (1993).
34) Koo, T. S., Kim, D. H., Ahn, S. H., Kim, K. P., Kim, I. W., Seo, S. Y., Suh, Y. G., Kim, D. D., Shim, C. K. and Chung, S. J.: Comparison of pharmacokinetics of loxoprofen and its active metabolites after an intravenous, intramuscular, and oral administration of loxoprofen in rats: evidence for extrahepatic metabolism. *J. Pharm. Sci.*, **94**: 2187–2197 (2005).

1521-0103/345/2/271–283$25.00
THE JOURNAL OF PHARMACOLOGY AND EXPERIMENTAL THERAPEUTICS

http://dx.doi.org/10.1124/jpet.112.201814
J Pharmacol Exp Ther 345:271–283, May 2013

Long-Acting Human Serum Albumin-Thioredoxin Fusion Protein Suppresses Bleomycin-Induced Pulmonary Fibrosis Progression

Ryota Tanaka, Hiroshi Watanabe, Azusa Kodama, Victor Tuan Giam Chuang, Yu Ishima, Keisuke Hamasaki, Ken-ichiro Tanaka, Tohru Mizushima, Masaki Otagiri, and Toru Maruyama

Department of Biopharmaceutics, Graduate School of Pharmaceutical Sciences (R.T., H.W., A.K., Y.I., K.H., T.Ma.), and Center for Clinical Pharmaceutical Sciences, School of Pharmacy, Kumamoto University, Chuo-ku, Kumamoto, Japan (H.W., Y.I., T.Ma.); School of Pharmacy, Faculty of Health Sciences, Curtin Health Innovation Research Institute, Curtin University, Perth, Western Australia, Australia (V.T.G.C.); Department of Analytical Chemistry, Faculty of Pharmacy, Keio University, Minato-ku, Tokyo, Japan (K.T., T.Mi.); and Faculty of Pharmaceutical Sciences and DDS Research Institute, Sojo University, Nishi-ku, Kumamoto, Japan (M.O.)

Received November 9, 2012; accepted February 26, 2013

ABSTRACT

Idiopathic pulmonary fibrosis (IPF) is thought to involve inflammatory cells and reactive oxygen species (ROS), such as superoxide anion radical ($O_2^{\cdot-}$). There is currently no effective treatment of IPF. We previously developed a human serum albumin (HSA)–thioredoxin 1 (Trx) fusion protein (HSA-Trx) designed to overcome the unfavorable pharmacokinetic and short pharmacological properties of Trx, an antioxidative and anti-inflammatory protein. In this study, we examined the therapeutic effect of HSA-Trx on an IPF animal model of bleomycin (BLM)-induced pulmonary fibrosis. A pharmacokinetic study of HSA-Trx or Trx in BLM mice showed that the plasma retention and lung distribution of Trxc was markedly improved by fusion with HSA. A weekly intravenous administration of HSA-Trx, but not Trx, ameliorated BLM-induced fibrosis, as evidenced by a histopathological analysis and pulmonary hydroxyproline levels. HSA-Trx suppressed active-transforming growth factor (TGF)-β levels in the lung and inhibited the increase of inflammatory cells in bronchoalveolar lavage fluid, pulmonary inflammatory cytokines, and oxidative stress markers. An in vitro EPR experiment using phosphate-buffered saline–stimulated neutrophils confirmed the $O_2^{\cdot-}$ scavenging ability of HSA-Trx. Furthermore, post-treatment of HSA-Trx had a suppressive effect against BLM-induced fibrosis. These results suggest that HSA-Trx has potential as a novel therapeutic agent for IPF, because of its long-acting antioxidative and anti-inflammatory modulation effects.

Introduction

Idiopathic pulmonary fibrosis (IPF) is a chronic fibrosing interstitial pneumonia with no identifiable cause. It remains a devastating disease, with a 5-year mortality rate of 50% because of its insufficient response to medical therapy. Unfortunately, with the present lack of a complete understanding of the pathogenesis of IPF, the current treatment, which involves the use of steroids and immunosuppressants, does not improve the prognosis and recovery from the acute exacerbation of the disease (American Thoracic Society and the European Respiratory Society, 2000; Luppi et al., 2004). Therefore, the development of new drugs designed to suppress the progression of the disease or to prevent the acute exacerbation of IPF is of great importance.

Recent studies have suggested that oxidative stress plays an important role in the pathogenesis and development of IPF. In fact, increased level of reactive oxygen species (ROS), such as superoxide anion radical ($O_2^{\cdot-}$), and a decrease in the levels of glutathione and superoxide dismutase (SOD) in blood and in bronchoalveolar lavage fluid (BALF) in patients with IPF have been reported (Beeh et al., 2002; Psathakis et al., 2006). In addition, the genetic knockout of NADPH-oxidase, which increases the pulmonary level of $O_2^{\cdot-}$, resulted in the suppression of bleomycin (BLM)-induced pulmonary fibrosis in an IPF animal model. An intratracheal injection of BLM into the lungs of rodents causes alveolar cell damage, an inflammatory response, fibroblast proliferation, and subsequent collagen deposition, resembling human fibrotic lung disease (Moore and Hogaboam, 2008). In contrast, the genetic knockout of extracellular SOD, which decreases pulmonary ROS levels,

This research was supported by Japan Society for the Promotion of Science [Grant-in-Aid for Scientific Research KAKENHI 21390177]; and by Japan Science and Technology Agency, A-step feasibility study program [Grant 10801043].
dx.doi.org/10.1124/jpet.112.201814.

ABBREVIATIONS: 8-OH-dG, 8-hydroxy-2′-deoxygenase; BALF, bronchoalveolar lavage fluid; BLM, bleomycin; DMPO, 5,5-dimethyl-1-pyrroline *N*-oxide; ELISA, enzyme-linked immunosorbent assay; H&E, hematoxylin and eosin; HSA, human serum albumin; HSA-Trx, human serum albumin-thioredoxin 1 fusion protein; IL, interleukin; IPF, idiopathic pulmonary fibrosis; MDA, malondialdehyde; MIF, migration inhibitory factor; NO_2-Tyr, nitrotyrosine; OCT, optimal cutting temperature; PBS, phosphate-buffered saline; PMA, phorbol 12-myristate 13-acetate; ROS, reactive oxygen species; SOD, superoxide dismutase; TCA, trichloroacetic acid; TNF, tumor necrosis factor; Trx, thioredoxin 1.

resulted in the progression of the BLM-induced pulmonary fibrosis (Fattman et al., 2003; Manoury et al., 2005). On the other hand, the role of chronic inflammation in the pathogenesis of IPF has been the focus of a number of studies, in view of the presence of interstitial and alveolar inflammatory cells and the expression of inflammatory cytokines in the lungs of patients with IPF (Keane and Strieter, 2002). The findings of a large prospective study examining the histopathologic variability of surgical lung biopsies in 109 patients with IPF suggest an evolving disease process with chronic inflammation playing a pathogenic role (Flaherty et al., 2001). In addition, it has been well established that the levels of inflammatory cytokines and chemokines, especially interleukin (IL)-6, tumor necrosis factor (TNF)-α, and migration inhibitory factor (MIF), are markedly increased in the lungs of BLM-induced disease model animals, and it has also been reported that the knockout of IL-6 or the administration of anti-TNF-α or MIF antibodies suppress BLM-induced lung disorders (Piguet et al., 1989, 1993; Tanino et al., 2002; Chaudhary et al., 2006; Saito et al., 2008). Therefore, drugs with both antioxidative and anti-inflammatory properties would be expected to be useful in the treatment of IPF.

Thioredoxin-1 (Trx) is a small redox-active protein (M_r of ~12 kDa) that is ubiquitously present in the human body and is one of the defense proteins induced in response to various oxidative stress conditions (Holmgren, 1989; Nakamura et al., 2005). In addition to its potent antioxidative effect, which is derived from dithiol-disulfide exchange in its active site, Trx also has anti-inflammatory properties, mainly because of its ability to inhibit neutrophil chemotaxis to inflammatory sites and to suppress the expression and activation of the macrophage MIF (Nakamura et al., 2001; Tamaki et al., 2006). Because of its desirable antioxidative and anti-inflammatory properties, Trx represents a new and potentially effective therapeutic agent for the treatment of IPF. However, because Trx is eliminated extensively via glomerular filtration, its plasma half-life is only approximately 1 hour in mice and 2 hours in rats, which is extremely short in terms of producing a significant therapeutic impact (Nakamura et al., 2001; Ueda et al., 2006). To obtain a satisfactory therapeutic outcome, a sustainable therapeutic concentration of Trx would be needed. To achieve this, constant infusion or frequent repeated administrations of Trx would be required (Hoshino et al., 2003; Liu et al., 2004; Ueda et al., 2006). Hoshino et al. (2003) demonstrated that exogenous recombinant Trx was effective in inhibiting BLM-induced lung damage when administered intraperitoneally or via a continuous infusion of Trx that is repeated at 2-day intervals.

In an attempt to increase the blood retention time of Trx, we recently produced a genetically engineered fusion protein of human serum albumin (HSA) and Trx (HSA-Trx) with use of a *Pichia* expression system. The plasma half-life of the HSA-Trx fusion protein in normal mice was found to be similar to that of HSA, which is 10 times longer than the plasma half-life of Trx (Ikuta et al., 2010). Of interest, HSA-Trx showed a higher distribution to the lungs than did Trx. Therefore, a further attempt will be made to investigate the clinical usefulness of HSA-Trx in treating oxidative stress and inflammation-related lung disorders.

The purpose of this study was to investigate the therapeutic impact of HSA-Trx in the treatment of IPF. With use of the BLM-induced pulmonary fibrosis animal model, the results showed that HSA-Trx could prevent BLM-induced pulmonary fibrosis through its long-acting antioxidative and anti-inflammatory modulation effects.

Materials and Methods

BLM was purchased from Nippon Kayaku (Tokyo, Japan). Mayer's hematoxylin, a 1% eosin alcohol solution, mounting medium for histologic examinations (malinol), and Masson's trichrome staining reagents were from Muto Pure Chemicals (Tokyo, Japan). Optimal cutting temperature (OCT) compound was purchased from Sakura Finetek (Tokyo, Japan). Chloral hydrate, chloramine T, and phorbol 12-myristate 13-acetate (PMA) were obtained from Sigma-Aldrich (Tokyo, Japan). Paraformaldehyde, trichloroacetic acid (TCA), perchloric acid, and 4-(dimethylamino)-benzaldehyde were from Nacalai Tesque (Kyoto, Japan). Diethylene-triamine-pentaacetic acid was purchased from Dojindo Laboratories (Kumamoto, Japan); 5,5-dimethyl-1-pyrroline *N*-oxide (DMPO) was purchased from Alexis Biochemicals (Lausen, Switzerland). The TGF-β1 enzyme-linked immunosorbent assay (ELISA) kit was purchased from R&D Systems Inc. (Minneapolis, MN). IL-6 and TNF-α ELISA kit were purchased from Biolegend (San Diego, CA). Sea-ICR mice (age, 6 weeks; male) were obtained from Kyudo Co., Ltd. (Saga, Japan). Other chemicals used were obtained from commercial suppliers.

Production of HSA-Trx Fusion Protein. Trx and HSA fusion protein was produced in accordance with the method reported previously (Ikuta et al., 2010; Furukawa et al., 2011) with a slight modification. The transformed *Pichia pastoris* was incubated in 1.25 liters of growth phase media, BMGY (1% yeast extract, 2% peptone, 100 mM potassium phosphate [pH 6.0], 1.34% yeast nitrogen base with ammonium sulfate without amino acids, 4×10^{-5} % biotin, 1% glycerol) for 2 days (OD_{600} = 2). It was then cultured in 800 ml of protein induction phase media, BMMY (1% yeast extract, 2% peptone, 100 mM potassium phosphate [pH 6.0], 1.34% yeast nitrogen base with ammonium sulfate without amino acids, 4×10^{-5} % biotin, 1% methanol) for 3 days at 30°C. Methanol was added every 24 hours so that the concentration of methanol was maintained at 1% to sustain the protein expression induction effect. The secreted fusion protein was isolated from the growth media as follows. The solution was loaded on to a column of Blue Sepharose 6 Fast Flow column (GE Healthcare, Tokyo, Japan) equilibrated with 200 mM sodium acetate buffer (pH 5.5) after the medium was dialyzed against the same buffer. The column was washed with ~5 bed volumes of 200 mM sodium acetate buffer (pH 5.5), and then the fusion protein was eluted with 20 mM sodium acetate buffer (pH 6.5) containing 3 M NaCl. Next, with use of AKTA prime, the eluate was loaded onto a column of 5-ml HiTrap Phenyl HP column (GE Healthcare) for hydrophobic chromatography with the following conditions (buffer A, 0 mM Tris-HCl/1.5 M ammonium sulfate [pH 7.0]; buffer B, 50 mM Tris-HCl [pH 7.0]; gradient, 0–100% [buffer B] 100 ml; flow rate, 3 ml/min). The desired fusion protein was obtained by delipidation with activated carbon treatment, as described by Chen (1967). The fusion protein was analyzed using SDS-PAGE and native SDS-PAGE using a 15% polyacrylamide gel, with Coomassie Blue R250 staining. The purity of the fusion protein was estimated to be more than 95% (Ikuta et al., 2010).

Production of BLM-Induced Pulmonary Fibrosis Mice Model. All animal experiments were conducted in accordance with the guidelines of Kumamoto University for the care and use of laboratory animals. BLM-induced pulmonary fibrosis model mice were produced by intratracheal injection of BLM (5 mg/kg) in phosphate-buffered saline (PBS; 1 ml/kg) under anesthesia with chloral hydrate (500 mg/kg) on day 0 (Tanaka et al., 2010). Either Trx or HSA-Trx was administered (but not both) intravenously (3.5 nmol protein in 200 μl PBS/mouse) via the mouse tail vein 30 minutes before BLM treatment (day 0). HSA-Trx was administered intravenously on days 0 and 7 (refer to every 1 week, Fig. 1A) or only on day 0 (refer to every 2 weeks, Fig. 1A). For an intervention study, the first dose of HSA-Trx was administered 1 day after the BLM treatment, and the subsequent dose was administered on day 7 after the BLM treatment. (Fig. 1C).

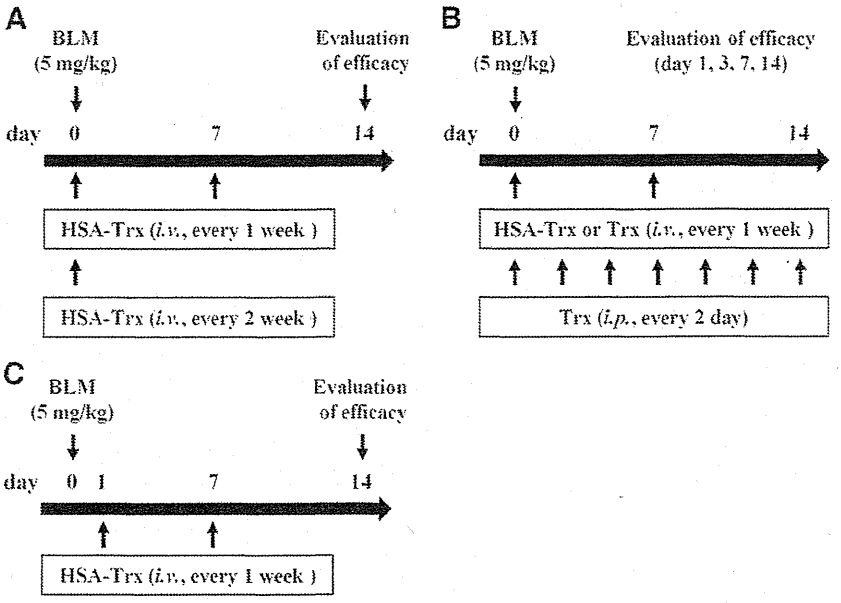

Fig. 1. Schematic summary of the experimental protocol for evaluating the effect of HSA-Trx on BLM-induced pulmonary fibrosis used in the study. HSA-Trx was administrated intravenously on days 0 and 7 (every 1 week; A) or only on day 0 (every 2 weeks; A). On day 0, HSA-Trx was administered 30 minutes before BLM treatment. For the intervention study, the first dose of HSA-Trx was administered 1 day after BLM treatment, and the subsequent dose was administered at day 7 after BLM treatment (C).

Histopathological Analysis of Lung Tissue (Hematoxylin and Eosin Staining and Masson's Trichrome Staining of Collagen). On day 14 after BLM administration, the whole lungs were flushed with 4% paraformaldehyde before being removed. The removed lungs were fixed in 4% buffered paraformaldehyde and then embedded in paraffin before being cut into 4-μm-thick sections. For hematoxylin and eosin (H&E) staining, sections were stained first with Mayer's hematoxylin and then with 1% eosin alcohol solution. For Masson's trichrome staining, sections were sequentially treated with solution A [5% (wt/vol) potassium dichromate and 5% (wt/vol) TCA], Weigert's iron hematoxylin, solution B [1.25% (wt/vol) phosphotungstic acid and 1.25% (wt/vol) phosphomolybdic acid], 0.75% (wt/vol) Orange G solution, solution C [0.12% (wt/vol) xylidine Ponceau, 0.04% (wt/vol) acid fuchsin, and 0.02% (wt/vol) azophloxin], 2.5% (wt/vol) phosphotungstic acid, and finally an aniline blue solution. H&E and Masson's trichrome staining samples were mounted with malinol and inspected using a microscope (BZ-8000; Keyence, Osaka, Japan).

Determination of Lung Fibrosis. Fibrosis score was evaluated (×100) as the quantity of the section positively stained for collagen and displaying alveolar wall thickening (1 = <25%, 2 = 25–50%, 3 = 50–75%, and 4 = 75–100%) (Gibbons et al., 2011). Only fields in which most of the field was composed of alveoli were scored. The entire lung section was analyzed. The investigator was masked to each sample.

Determination of Hydroxyproline Level in Lung Tissues. Hydroxyproline content was determined as described previously (Woessner, 1961). On day 14 after BLM administration, the right lung was removed and homogenized in 1 ml of 5% TCA. After centrifugation, the pellets were hydrolyzed in 0.5 ml of 10 N HCl for 16 hours at 110°C. Each sample was incubated for 20 minutes at room temperature after the addition of 0.5 ml of 1.4% (wt/vol) chloramine T solution and then incubated at 65°C for 10 minutes after addition of 0.5 ml of Ehrlich's reagent (1 M DMBA, 70% [vol/vol] isopropanol and 30% [vol/vol] perchloric acid). The absorbance was measured at 550 nm to determine the amount of hydroxyproline.

Quantification of Activated TGF-β1, IL-6, and TNF-α and Western Blot Analysis of Macrophage MIF in Lung Tissue. On days 3 and 7 after BLM administration, the whole lungs were removed and homogenized in 0.5 ml of buffer (PBS, 1% protease inhibitor cocktail, 10 mM EDTA, 0.05% Tween 20). After centrifugation at 21,000*g* for 10 minutes at 4°C (two times), the supernatants were recovered. The amounts of active TGF-β1 (day 7), IL-6, and TNF-α (days 3 and 7) in the supernatant were measured using ELISA, according to the manufacturer's protocol. In addition, Western blotting of MIF chemokine in the supernatant was performed using the following protocol. After measurement of the protein content with use of the BCA protein assay reagent (Pierce Biotechnology Inc., Rockford, IL), each sample was separated by 12.5% SDS-PAGE and transferred onto polyvinylidene difluoride membranes (Immobilon-P; Millipore, Bedford, MA) by wet electroblotting. The membranes were blocked for 1 hour at room temperature with 5% skim milk in PBS. The membranes were washed three times with PBS containing 0.05% Tween 20 (PBS-T) and incubated for 2 hours at room temperature with a 400 ng/ml primary mouse monoclonal antibody against N terminus of MIF of human origin, which has cross-reactivity with mouse MIF (sc-271631; Santa Cruz Biotechnology Inc., Santa Cruz, CA) in PBS-T. The membranes were washed 3 times with PBS-T and incubated with the secondary antibody (horseradish peroxidase-linked anti-mouse IgG [H+L]; Invitrogen, Carlsbad, CA) for 1.5 hours at room temperature. The membranes were washed 3 times with PBS-T, and immunoblots were visualized using the SuperSignal West Pico chemiluminescent substrate (Pierce Biotechnology Inc.) with LAS-4000EPUVmini (Fujifilm, Tokyo, Japan).

Counting of Cells in BALF. On days 1 and 3 after BLM administration, the mice were anesthetized with pentobarbital, the chests were opened, and blood was drained. BALF samples were collected by cannulating the trachea and lavaging the lung with 1 ml of sterile PBS containing 50 U/ml heparin (two times). Approximately 1.8 ml of BALF was routinely recovered from each animal. The BALF was centrifuged at 4100*g* for 5 minutes at 4°C to separate the cells in the BALF from the liquid. Cells were dissolved in 0.9% NaCl, and lysate was centrifuged again. From the recovered cells, the total cell number was counted using a hemocytometer. Cells were stained with Diff-Quick reagents (Kokusai Shiyaku, Kobe, Japan), and the ratios of alveolar macrophages, neutrophils, and lymphocytes to total cells were determined. More than 200 cells were counted for each sample.

Immunostaining of Lungs Tissue. On day 3 after BLM administration, the whole lungs were flushed with sterile PBS before being removed. The removed lungs were stored in 4% paraformaldehyde at 4°C for 2 hours before being immersed in a 10% sucrose solution overnight. The concentration of sucrose solution was then adjusted to 20% at room temperature, and incubation was continued for another 6 hours. The recovered lungs were covered with OCT compound and frozen at −80°C. Next, the lungs frozen with cryostat (CM3000II; Leica, Wetzlar, Germany) were sliced at a thickness of 4 μm and attached on a glass slide. The slide was then cleansed to remove OCT compound and dried. After drying the slide completely,

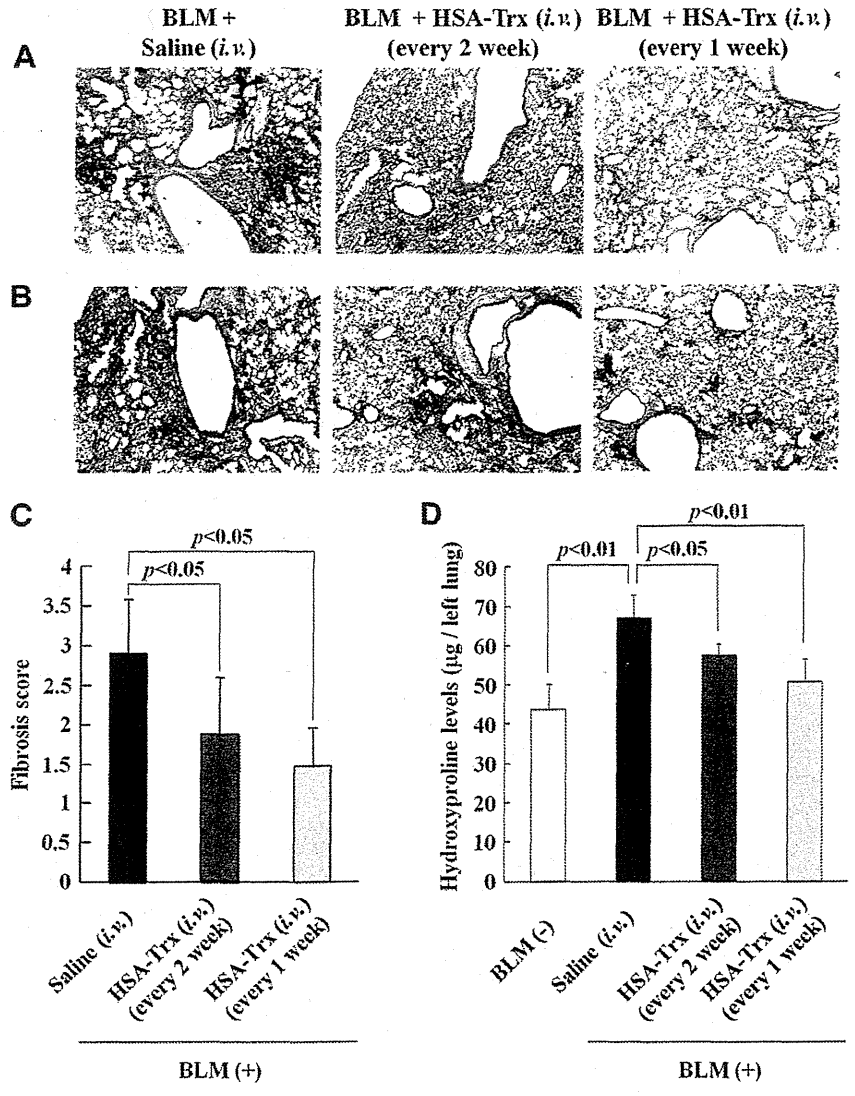

Fig. 2. Effect of HSA-Trx (intravenously; every 2 weeks or every 1 week) on the BLM-induced pulmonary fibrosis. (A and B) Sections of pulmonary tissue were prepared 14 days after BLM administration and subjected to histopathological examination [H&E (A) and Masson's trichrome staining (B)]. (C) Fibrosis score was evaluated as the quantity of the section positively stained for collagen and displaying alveolar wall thickening. (D) Hydroxyproline levels in lung were determined 14 day after BLM administration. Each bar represents the mean ± S.D. (C, n = 3–5; D, n = 5).

a solution containing 50 mM Tris/HCl + 0.1% Tween 20 (T-TB) was used to solubilize the lung slice, followed by blocking with Block Ace (Dainippon Pharmaceutics, Osaka, Japan) at room temperature for 15 minutes. Next, the primary antibody reaction was conducted below 4°C overnight. In addition, the primary mouse monoclonal antibody against 8-hydroxy-2′-deoxygenase (8-OH-dG) [15A3] (sc-66036; Santa Cruz Biotechnology Inc.), which has cross-reactivity with mouse, or the primary rabbit polyclonal antibody against nitrotyrosine (NO_2-Tyr;AB5411; Millipore, Billerica, MA), which has cross-reactivity with mouse, was diluted to 2 or 20 μg/ml before use, respectively. The lung slices were then washed with 50 mM Tris/HCl (TB) and T-TB, followed by the secondary antibody reaction at room temperature for 1.5 hours. For the secondary antibody, in relation to NO_2-Tyr and 8-OH-dG, Alexa Fluor 546 goat anti-mouse IgG (H+L; Invitrogen) and Alexa Fluor 488 goat anti-mouse IgG (H+L; Invitrogen) diluted 200 times were respectively used. After the reaction, the slide was observed using a microscope (BZ-8000; Keyence). Image analyses of the extent and intensity of 8-OH-dG and NO_2-Tyr staining were also performed using ImageJ software.

Determination of Malondialdehyde in Lung Tissue. On day 3 after BLM administration, the right lung was removed and homogenized in 0.5 ml of radioimmunoprecipitation assay/PI buffer (150 mM NaCl, 1% Nonidet P-40, 10 mM Tris-HCl, pH 7.4, including a 1% solution of a protease inhibitor; Nacalai Tesque, Tokyo, Japan). After centrifugation, the amount of malondialdehyde (MDA) in supernatant was measured using thiobarbituric acid reactive substances assay kit (Cayman Chemical, Ann Arbor, MI), which is a well-established method for measuring lipid peroxidation, according to the manufacturer's protocol.

Isolation of Polymorphonuclear Neutrophils. Whole blood was obtained from 10 mice. Heparinized blood was mixed with an equal volume of 3% dextran in 0.9% NaCl. After 30 minutes of gravity sedimentation, the upper layer, containing leukocytes, was removed and centrifuged at 620g for 10 minutes. The cell pellet was resuspended in 0.9% NaCl and underlaid with Ficoll-Paque (GE Healthcare). After centrifugation for 30 minutes at 1490g, the mononuclear cell layer was isolated, and contaminating red blood cells were removed by hypotonic lysis. After centrifugation for 10 minutes at 760g (two times), the pellet was resuspended, and the neutrophils were plated at 1.0×10^6 cells/ml in PBS.

Measurement of Neutrophil-Derived ROS. The scavenging activity of HSA-Trx against O_2^- released from neutrophils was determined using EPR spin trapping with DMPO. The neutrophils (1.0×10^6 cells/ml) were pretreated with PMA (1 μg/ml) for 7 minutes at 37°C to activate the cells and generate ROS. Aliquots of this cell suspension were combined with 100 μM DTPA in Hanks' balanced salt solution in the absence or presence of either HSA-Trx (10, 30, 50 μM), HSA (30 μM), or Trx (30 μM). After activation of neutrophils,

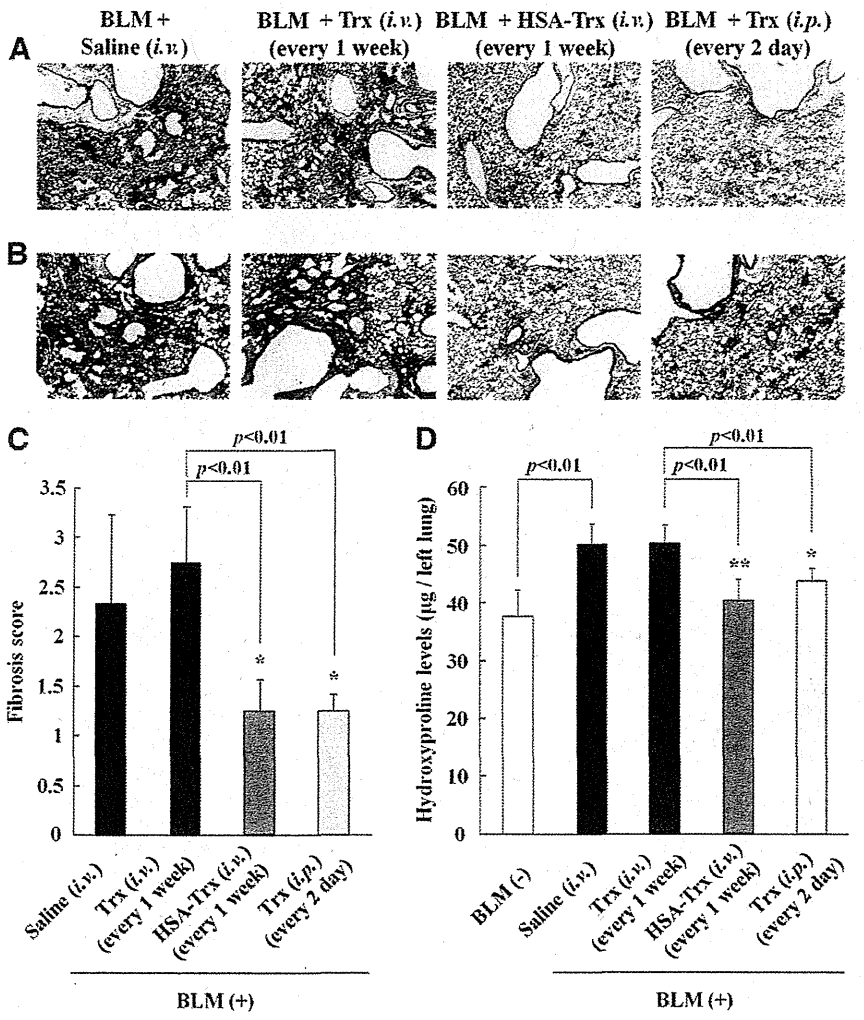

Fig. 3. Effects of HSA-Trx (intravenously; every 1 week), Trx (intravenously; every 1 week), or Trx (intraperitoneally; every 2 days) on the BLM-induced pulmonary fibrosis. (A and B) Sections of pulmonary tissue were prepared 14 days after BLM administration and subjected to histopathological examination ([A] H&E and [B] Masson's trichrome staining). (C) Fibrosis score was evaluated as the quantity of the section positively stained for collagen and displaying alveolar wall thickening. (D) Hydroxyproline levels in lung were determined 14 days after BLM administration. Each bar represents the mean ± S.D. (C, $n = 4$; D, $n = 5$). $^{**}P < 0.01$; or $^{*}P < 0.05$ versus BLM(+), saline (i.v.).

this reaction mixture was added with DMPO (27 mM). After 6 minutes of addition of DMPO, EPR spectra were recorded at room temperature in a JES-TE-200 spectrometer (JEOL, Tokyo, Japan) under the following conditions: modulation frequency, 100 kHz; microwave frequency, 9.43 GHz; microwave power, 40 mW; scanning field, 335.2 ± 5 mT; sweep time, 2 minutes; field modulation width, 0.25 mT; receiver gain, 630; and time count, 0.3 seconds.

Radiolabeling of Proteins with ^{125}I. HSA-Trx and Trx were radiolabeled with ^{125}I according to the procedures reported previously (Watanabe et al., 2001; Furukawa et al., 2011) and purified using a Pharmacia Bio-Gel PD-10 column. The radiolabeled proteins were diluted with nonlabeled protein before conducting the pharmacokinetic experiments to adjust the dose (mg/kg) of protein in each group.

Pharmacokinetics of Trx and HSA-Trx in BLM Mice. On day 14 after BLM administration, the ^{125}I proteins (0.1 mg/kg) were injected into the tail vein of mice (~10^5 cpm/mouse). Approximately 500 μl of blood was collected from the vena cava at 0.05, 0.167, 0.5, 1, 2, 4, 6, and 12 hours after the injection of these radiolabeled proteins with the mice under ether anesthesia, and plasma was obtained. Degraded proteins and free ^{125}I were removed from plasma by centrifugation in 1% bovine serum albumin and 40% TCA. At each of these time points, the mice were sacrificed. The organs were rinsed with saline and weighed, and the ^{125}I radioactivity contained in each tissue was determined using a gamma-counter (ARC-5000; Hitachi Aloka Medical, Tokyo, Japan).

Data Analysis. Noncompartment model was used in the pharmacokinetic analyses after ^{125}I proteins administration. Each parameter was calculated using the program MOMENT (BS) (Tabata et al., 1996). Data are means ± S.D. for the indicated number of animals. Significant differences among each group were examined using a one-way of analysis of variance followed by Tukey's multiple comparison. A probability value of $P < 0.05$ was considered to indicate statistical significance.

Results

Evaluation of the Administration Schedule of HSA-Trx in BLM-Induced Pulmonary Fibrosis. Pulmonary fibrosis was induced in mice by a single intratracheal administration of BLM (day 0). Because Hoshino et al. (2003) found that the multiple administration of Trx (3.5 nmol/body) prevented BLM-induced pulmonary fibrosis, we adopted a dose of HSA-Trx equivalent to one Trx treatment (3.5 nmol/body). Figure 1 shows a schematic summary of the experimental protocols used in the study. The effect of HSA-Trx on BLM-induced pulmonary fibrosis was evaluated using H&E staining (Fig. 2A), Masson's trichrome staining (Fig. 2B), the quantity analysis of the section positively stained for collagen (Fig. 2C), and the measurement of hydroxyproline levels in lung tissue (Fig. 2D) on day 14.

H&E staining showed that BLM administration induced severe lung damage (thickened and edematous alveolar walls

and interstitia) and the infiltration of inflammatory cells into these regions (Fig. 2A). Masson's trichrome staining of collagen and the measurement of hydroxyproline levels in lung tissue indicated that BLM induced the deposition of collagen in lung (Fig. 2, B–D). These phenomena induced by BLM were all significantly suppressed by the HSA-Trx treatment. In addition, the administration of HSA-Trx at weekly intervals had a more potent effect than its use at 2-week intervals (Fig. 2, A–D). Therefore, HSA-Trx was administered once per week in the subsequent experiments.

Effect of HSA-Trx on Histologic Alterations and Hydroxyproline Levels in Lung Tissue. Hoshino et al. (2003) demonstrated that, when Trx is administered every 2 days, it prevents BLM-induced pulmonary fibrosis. Thus, we compared the effect of the intravenous administration of HSA-Trx at weekly intervals with that for the intravenous administration of Trx at weekly intervals or the intraperitoneal administration of Trx at 2-day intervals (Fig. 1B).

H&E staining (Fig. 3A), Masson's trichrome staining (Fig. 3B), the quantity analysis of the section positively stained for collagen (Fig. 3C), and hydroxyproline levels in lung tissue (Fig. 3D) clearly indicated that HSA-Trx, when administered at 1-week intervals, significantly suppressed the lung injury and fibrosis in diseased model mice. Intraperitoneal administration of Trx at 2-day intervals resulted in similar therapeutic effects as those for the HSA-Trx treatment at weekly intervals, but intravenous administration of Trx at weekly intervals showed no suppressive effect.

Effect of HSA-Trx on Active TGF-β1 Levels in Lung Tissue. TGF-β1 plays an important role in BLM-induced pulmonary fibrosis (Kinnula et al., 2005; Chaudhary et al., 2006). To reveal the mechanism underlying the suppressive effect of HSA-Trx on BLM-induced pulmonary fibrosis, the levels of active TGF-β1 in lung tissue on day 7 were determined. As shown in Fig. 4, the level of active TGF-β1 was increased in BLM mice [BLM(+), saline (i.v.)]. In contrast, HSA-Trx decreased the level of active TGF-β1 to the same level as the normal group [BLM(−)].

Effect of HSA-Trx on BALF Cells. To evaluate the effects of HSA-Trx on the inflammatory response induced by BLM, the cells in BALF were analyzed. As shown in Fig. 5, the administration of BLM resulted in an increase in the number of inflammatory cells (Fig. 5A), including alveolar macrophages (Fig. 5B), neutrophils (Fig. 5C), and lymphocytes (Fig. 5D) on days 1 and 3 after BLM administration. The HSA-Trx treatment significantly reduced the number of total cells and neutrophils on both days 1 and 3 and alveolar macrophages and lymphocytes on day 3. These results suggest that HSA-Trx ameliorates the BLM-induced pulmonary inflammatory response.

Effect of HSA-Trx on Inflammatory Cytokines and Chemokine Levels in Lung Tissue. We also examined the effect of HSA-Trx on IL-6, TNF-α, and MIF levels in the lung tissue of BLM-induced pulmonary fibrosis on days 3 and 7. As shown in Fig. 6, the levels of IL-6 (Fig. 6A), TNF-α (Fig. 6B), and MIF (Fig. 6, C and D) in lung tissue that were increased by BLM were significantly decreased as the result of the HSA-Trx treatment. These data suggest that HSA-Trx exerts an anti-inflammatory action against BLM-induced pulmonary damage.

Effect of HSA-Trx on Oxidative Stress in Lung Tissue. Recently reported findings suggest that ROS released from activated leukocytes, especially alveolar macrophages and neutrophils,

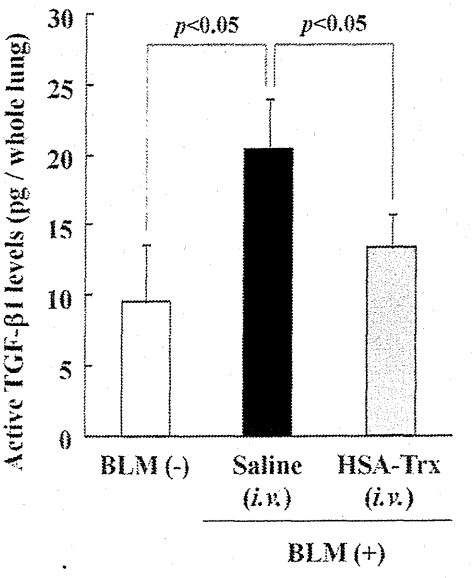

Fig. 4. Effect of HSA-Trx on active TGF-β1 levels in BLM mouse lung. Active TGF-β1 levels in lung were determined 7 days after BLM administration. Each bar represents the mean ± S.D. (n = 5).

are associated with the development of BLM-induced lung injury (Manoury et al., 2005). To evaluate the effect of HSA-Trx on the oxidative stress induced by BLM in the lung, immunostaining of 8-OH-dG and NO_2-Tyr, oxidized product of nucleic acids and proteins, respectively, and also quantification of lipoperoxidation final reaction substances, MDA, in lung sections were performed on day 3 after BLM administration. As shown in Fig. 7, the accumulation of 8-OH-dG, NO_2-Tyr, and MDA in lung tissue increased in BLM-mice [BLM(+), saline (i.v.)], compared with normal mice [BLM(−)], whereas HSA-Trx clearly suppressed the levels of these oxidative stress markers in the lungs.

To confirm whether HSA-Trx shows scavenging activity against $O_2^{\cdot-}$ generated from neutrophils, we conducted ex vivo EPR spectroscopy with use of a DMPO spin-trapping technique. As shown in Fig. 8, although PMA-stimulated neutrophils generated $O_2^{\cdot-}$ and increased EPR signaling, HSA-Trx significantly decreased the EPR signaling in a concentration-dependent manner (Fig. 8, A and B). We also compared the $O_2^{\cdot-}$ scavenging activity among HSA-Trx, Trx, and HSA. At a 30 μM concentration of each protein, HSA-Trx and Trx significantly decreased the EPR signal by 40 and 85%, respectively, whereas HSA alone did not significantly change the intensity of the signal (Fig. 8, C and D).

Effect of Post-Treatment of HSA-Trx on BLM-Induced Pulmonary Fibrosis. For future clinical applications, the postadministration effect of HSA-Trx against BLM-induced fibrosis was examined (Fig. 1C). Because HSA-Trx suppressed ROS production by neutrophils (Fig. 8), the effect of the postadministration of HSA-Trx was examined at 1 and 7 days after BLM treatment, when a marked increase in neutrophils in BALF was observed (Fig. 5C). The results of H&E staining (Fig. 9A), Masson's trichrome staining (Fig. 9B), the quantity analysis of the section positively stained for collagen (Fig. 9C), and the determination of hydroxyproline levels (Fig. 9D) on day 14 showed that the post-treatment of HSA-Trx suppressed the progression of BLM-induced fibrosis.